1-1-2016

Integrated PHEV Charging Loads Forecasting Model and Optimization Strategies

Yin Yao
University of Denver

Integrated PHEV Charging Loads Forecasting Model and Optimization Strategies

_____

A Dissertation

Presented to

the Faculty of the Daniel Ritchie School of Engineering and Computer Science

University of Denver

_____

In Partial Fulfillment

of the Requirements for the Degree

Doctor of Philosophy

_____

by

Yin Yao

November 2016

Advisor: David Wenzhong Gao

Author: Yin Yao
Title: Integrated PHEV Charging Loads Forecasting Model and Optimization Strategies
Advisor: David Wenzhong Gao.
Degree date: November 2016

Abstract

In this dissertation, an integrated Plug-in Electric Vehicle (PHEV) charging loads forecasting model is developed for regular distribution level system and microgrid system. For regular distribution system, charging schedule optimization is followed up. The objectives are 1. Better cooperation with renewable energy sources (especially wind). 2. Relieving the pressure of current distribution transformers in condition of high penetration level PHEVs. As for microgrid, renewable energy power plants (wind, solar) plays a more important role than regular system. Due to the fluctuation of solar and wind plants' output, an empirical probabilistic model is developed to predict their hourly output. On the other hand, PHEVs are not only considered at the charging loads, but also the discharging output via Vehicle to Grid (V2G) method which can greatly affect the economic dispatch for all the micro energy sources in microgrid. Optimization is performed for economic dispatch considering conventional, renewable power plants, and PHEVs. The simulation in both cases results reveal that there is a great potential for optimization of PHEVs' charging schedule. Furthermore, PHEVs with V2G capability can be an indispensable supplement in modern microgrid.

Acknowledgements

Thanks to my advisor, Dr. David Wenzhong Gao, Dr. Zhang for the great support and professional suggestions.

Table of Contents

List of Figures

List of Tables

Chapter 1. Introduction

1.1 Theoretical Background

In United States, there is a growing trend of PHEVs purchase due to their fuel efficiency and environmental friendliness. Electric motor is installed to improve the efficiency of traditional combustion engine and serves as an electric power output. Consequently, this type of vehicle contains hybrid power output from both combustion engine and electric motor. Large capacity battery packs are installed to extend the mileage in condition that the vehicle only relies on electricity. On/off board charger is equipped as well to make charging battery via home plug possible. If the amount of PHEVs grows as expected, future vehicles will be independent of petroleum, and PHEVs would become the mainstream vehicles.

The extra loads of PHEV battery charging will result in a load peak and increase the loss of life of transformer evidently. Obviously, dumb charging (V0G) will lead to the worst situation for transformer. There is a great potential to improve the aging problem by assigning an optimized starting charging time to each PHEV. The battery charging loads would be more evenly distributed.

With the trend of transportation electrification (hybrid, battery, and fuel cell vehicles), there is also a great potential for "vehicle-to-grid" (V2G) technology. V2G can be an indispensable supplement to the stability (voltage and frequency) and reliability of microgrid. Three vehicle types are defined in [1] that can supply power back to microgrid via V2G method, and the power markets which they can sell electricity to are also defined and explained. Under certain system condition, V2G can become a practical option in power market. For instance, V2G will not be a favorable option for baseload power, because baseload power can be dispatched economically with large traditional generators. V2G's greatest short-term objective is for quick-response, high-value electric services. These quick-response electric services are designed to smooth constant fluctuations in both generation (especially wind and solar farms) and demand sides. Another purpose of the introduction of V2G is to improve the robustness of system under unexpected equipment failures for system reliability consideration. The cost of quick-response electric service is $ 12 billion per year in the US (5-10% of total electric cost) [1].

Besides the advantages of V2G, compared with traditional generators, PHEVs' short operation hour and high cost per kWh of electric energy suggests that V2G power should be sold only to high-value, short-duration demands in power market.

There are several charging methods expected to be the mainstream methods for PHEVs in near future. These methods include centralized charging, self-motivated charging, battery swapping, etc.

Since the charging schedule of PHEVs is not predictable and they are allocated in different areas, the penetration of this large amount of PHEVs' charging load can be a great burden for microgrid in most conditions.

1.2 Motivation

After a new round of petroleum price increase, almost every aspect of our daily life is affected. For instance, the traveling cost of automobile and plane grows apparently. Consequently, cost of all kinds of merchandise increases. For every vehicle owner, more attention is paid to fuel efficiency to save money. As a result, the MPG (miles per gallon) value becomes an important criterion for customers who plan to purchase a new car. Commonly, for internal combustion engine vehicles, high MPG value usually means lower engine displacement, slow acceleration or compact size. To better utilize power from internal combustion engine, extra battery packs and electric motor are installed in

hybrid electric vehicles (HEV). These battery packs' capacity is much larger than that of current vehicle. They also get charged while internal combustion engine is working like normal vehicles. But, large capacity means it not only could power the air conditioner system, but also the electric motor for normal running. Less gasoline consumption also means less pollution to environment. This type of vehicles possesses two engines, combustion engine and electric motor. But all power comes from gasoline. This type of HEV is called conventional hybrid electric vehicle.

As to conventional hybrid electric vehicles, the most popular one should be Toyota Prius. Prius is the first type of hybrid vehicle that put into large-scale production in 1997. In 2001, Prius was sold to over 40 countries all over the world. Her largest market now is United States. The success of Prius reveals a bright future for hybrid electric vehicles. Hybrid electric vehicles have two or even more energy sources. For Prius, they are combustion engine and electric motor. Other energy sources, such as hydrogen and fuel cell battery, are also options in future. Compared to hybrid electric vehicles, they are still in research stage. In recent years, engineers are trying to install more battery packs in hybrid electric vehicles and let these batteries be charged from the grid with the help of on/off board charger. This new type of hybrid electric vehicle is called Plug-in Hybrid Electric Vehicle (PHEV). In next two decades, it is hoped that automobiles will continuously become independent of petroleum, and PHEVs will replace conventional combustion engine vehicles gradually.

That oil resource is going to be exhausted is part of the reason. Besides, greenhouse gas output from combustion-engine vehicles is a serious threat to the environment, especially to the Atmosphere. Global warming is the most harmful phenomenon due to carbon gas output. Pure electric vehicle does not generate any carbon dioxide. They are friendlier to environment than conventional ones. If electricity is from renewable-energy power plant, the output of carbon dioxide could be further decreased. There have been many studies about PHEVs' impacts on current power grid. These can be classified as vehicle performance studies, supply adequacy, Vehicle to Grid (V2G) studies and distribution system impact studies. This project is primarily focused on large-scale PHEVs' integration into power grid as charging loads and potential effects for the operation of the rid.

1.3 Dissertation Organization

In this dissertation, an integrated Plug-in Electric Vehicle (PHEV) charging loads forecasting model is developed for regular distribution level system and microgrid system. For regular distribution system, charging schedule optimization is followed up. The objectives are 1. Better cooperation with renewable energy sources (especially wind). 2. Relieving the pressure of current distribution transformers in condition of high penetration level PHEVs. As for microgrid, renewable energy power plants (wind, solar) plays a more important role than regular system. Due to the fluctuation of solar and wind plants' output, an empirical probabilistic model is developed to predict their hourly

output. On the other hand, PHEVs are not only considered at the charging loads, but also the discharging output via Vehicle to Grid (V2G) method which can greatly affect the economic dispatch for all the micro energy sources in microgrid. Optimization is performed for economic dispatch considering conventional, renewable power plants, and PHEVs. The simulation in both cases results reveal that there is a great potential for optimization of PHEVs' charging schedule. Furthermore, PHEVs with V2G capability can be an indispensable supplement in modern microgrid.

Chapter 2. Literature Review

There have been a lot of studies about PHEVs. The main categories are vehicle performance studies, supply adequacy, Vehicle to Grid (V2G) studies, and distribution system impact studies. For example, a stochastic method was developed in [2] to simulate the charging loads of PHEVs in China. An optimization of charging pattern was introduced in [3] considering distribution grid constraints. For integration of PHEV charging and renewable energy, the study is mainly focused on utilization of surplus wind power. A new control method for the wind power/battery energy storage system is discussed in [4] to smooth out the fluctuation of wind farm (WF) output. In [5], a coordinated approach of wind power and PHEVs charging in market aspect was developed. As for the V2G study, the integration of V2G to wind farms is discussed in [34]. In [36], the impact of V2G to residential distribution network is evaluated and analyzed. From [31], V2G can not only stabilize the existing power system, but also support large scale of renewable energy plants. Finally, case study of Western Danish Power system is considered in [32] to evaluate the performance of V2G

Chapter 3. PHEV Charging Load Forecast Model

Referring to wind forecasting models [6]-[7], PHEV charging load forecasting models can be classified according to time-scales or methodology. Three categories are classified depends on the length of the prediction time-scale.

1. Immediate-short-term (8 hours-ahead) forecasting
2. Short-term (day-ahead) forecasting
3. Long-term (multiple-days-ahead) forecasting

Besides time-scale classification, PHEV charging load forecasting models can be classified depends on their methodology as well. In current research, deterministic and statistic are two main approaches in forecast modelling.

- Deterministic approach (Physical approach)

Deterministic method is based on load prediction using actual vehicle 24-hour data like State of Charge (SOC), daily mileage, plug in/out time point. Since the data pool of PHEV charging load is extremely limited so far. These parameters are manually set according to traffic data [8] from combustion engine vehicles. Statistical approach

Statistical method is based on large amount of historical data without considering actual vehicle conditions. Artificial intelligence, such as neural or neuro-fuzzy network, can be utilized referring to wind forecasting [9]-[10]. In this disseration, due to the limited data pool of actual PHEV charging loads, an empirical probabilistic model is developed to predict hourly charging loads based on historical data from stochastic model which is explained in Chapter 1.

Table 1 Time-scale classification and possible applications

Time-scale	Range	Applications
Immediate-short-term	8 hours ahead	Real-time grid operations Regulation actions
Short-term	Day ahead	Economic dispatch planning Operational security in electricity market
Long-term	Multiple-days-ahead	Maintenance planning Operation management Optimal operation cost

Immediate-short-term forecasting is performed via statistical approach which require vast amount of historical data. With the amount of PHEVs keep growing, large amount of historical charging load data will be available. Artificial neural networks can be trained to utilize these data and make several hours ahead forecasting like WPMS immediate-short-term forecasting model which is used 95% territories of whole Germany to predict wind power production. Since the time scale is just several hours ahead, this forecast data can be a great reference for real-time operation and regulation actions.

For short/long-term forecasting, the prediction time-scale can be single/multiple days. With the increase of time scale, the forecasting model cannot just rely on historical data. It usually utilize both deterministic and statistic approach. This hybrid approach can be applied for economic dispatch and optimal operation cost. Hence, a hybrid stochastic model is developed in following section for optimal operation cost in regular distribution system and economic dispatch in microgrid.

- Hybrid stochastic model

Average daily mileage for private car is only about 42 miles for commuting to and from work or school [8]. In this dissertation, Chevy Volt is chosen as the model of mainstream family sedan. Taking into account safety factors, owner of PHEV should charge battery every two days at home or in workplace.

Private vehicle's main function is commuting. Therefore, charging period starts when they arrive at working places or arrive home. Since the aging of distribution transformer is the topic of this dissertation, only home charging period is considered. Workplace charging period is not included. It can be easily figured out that there is comparatively abundant charging time for private car. Therefore, for both periods, slow charging mode is the first option.

3.1 Stochastic Modeling for PHEVs

Charging patterns for PHEVs are affected by many factors, such as battery capacity, arrival and departure time, charging speed. So, it is better to define different charging patterns according to vehicle's function. In this project, all PHEVs are divided into two parts: public transportation vehicles and private vehicles.

- Public transportation vehicles

Public transportation plays a more and more indispensable role in traffic system. Therefore, this portion of traffic system should not be omitted even public buses do not constitute significant share of all vehicles in many cities in United States.

BYD electric bus is selected as the model because its electric driving capacity (EDC) is suitable for daily public bus operation. EDC is the miles that a PHEV could drive only from battery electricity, when its battery's state of charge is 100 percent. EDC of BYD electric bus is 155 miles in urban condition. Average daily mileage for normal transportation bus is about 90 to 125 miles [11]. So, electric bus is capable for a whole day operation without one charging. However, safety factor must be taken into consideration. Deeply charging the battery would harm its life. So, charging two times a day is essential. For school bus, daily mileage would be only one third of that of normal bus. Normal bus's operation hour begins at around 5:30 am and ends at 10:00 pm [11]. In rush hours, almost twice buses should be added to fleet. Commuting hour is 6:30 to 9:00 and 16:30 to 7:00 [11]. In commuting hour, time interval between two bus trips is

5~7 minutes. In contrast, time interval increases to 10 to 15 minutes in normal operation hour.

The first charging period begins at about 10 am and ends at 4:30 pm between two commuting-hour periods. Since the charging time is quite limited. C100D, a three phase charger, is used for this charging period. The power for C110D is 100 kW. It takes three hours for the on-board batteries to be fully charged [12]. Another charging period begins at 11:00 pm and ends at 5:30 am. One hour is reserved for daily preparation and dispatch. There is enough charging time at night. C60, 60kW three phase charger is used instead of C100D. The full-charge time is extended to 5 hours [12].

Table 2 Electric bus parameter [12]

Dimensions	Length	39.37 ft.
	Width	100.4 in
	Height	126.0 in
	Wheelbase	20.34 ft
	Track (F/R)	82.5/72.4 in
	Curb weight	30423.79 lb
	GVWR	39683.21 lb
	Seats	27+4 (foldable) +1 (driver)
	Wheelchair position	2
Performance	Top speed	62.1 mph
	Urban conditions	>= 155 mi
	Power consumption	120 kWh per 62 mi
	Turning radius	<40 ft
	Min ground clearance	5.5 in
	Approach/Departure angle	7 degrees/7 degrees
Chassis	Suspension	Front & rear self-levering air suspension, ECAS system
	Brakes	Front & rear disc-braking. ABS+ASR
	Steering	ZF8098 Electric hydraulic power steering gear
	Tires	Michelin 275/70R22.5
Motor	Type	Permanent magnet synchronous motor
	Max power	160 kW
	Rated power	110 kW
	Max torque	450Nm
Battery	Type	Fe battery
	Capacity	600 Ah
Charging equipment	C100D	three phase 480 plus/minus 10% charge voltage, 100 kW
	Charge time	3h
	C60	three phase 208 plus/minus 10% charge voltage, 60 kW
	Charge time	5h
Floor plan	Seats: 27 Seats + 4 Foldable + 1 Driver	

The starting state of charge (SOC) is assumed to follow a statistical normal distribution. SOC indicates the percentage of energy that remains in the battery. For

example, Cap is the capacity for vehicle's battery. The remaining energy in that battery is Cap × SOC. The battery capacity needed to be charged is Cap (i) × (1-SOC (i)).

For electric buses, when they come back to charging station, their SOC is generated according to equation (1). The expected average state of charge is set to 50% considering safety factor and life of battery. The standard deviation is set to 10%.

$$\begin{aligned} SOC_{Bus}^{m} &= random('norm', \mu, \sigma) \\ \mu_{Bus} &= 0.5 \\ \sigma_{Bus} &= 0.1 \end{aligned} \qquad (1)$$

Other parameters about time schedule for electric bus are summarized in Table 3.

Table 3 Time schedule for electric bus

Bus		
Average daily mileage	93-124 miles	
Operation time	5:30-6:00 to 22:00-23:00	
Peak periods	6:30-9:00	Commuting hour
	16:30-18:30	
Interval	3-5 minutes	Commuting hour
	7-8 minutes	Normal
Mileage capacity	155 miles	
Charging times	2 times a day	Take safety factor into consideration
Charging periods	10:00-16:30	Day time
	23:00-5:30	Night time
Starting SOC	Normal distribution N (0.5, 0.1)	

The arrival and departure time are also assumed to follow normal distribution. And the standard deviation is set to 45 minutes considering different arrival and departure times for different bus lines. Note that in one day, there are 1440 minutes. AT_{am}^{m} means the arrival time in am for the *m*-th electric bus in array. AT_{am}^{m} follows normal distribution, with a mean value of 600, corresponding to the 600th minute in 1440 minutes within a day. In other words, the average arrival time is 10:00 (600/60) am after morning commuting hour. Standard deviation is assumed to be 45 minutes. DT_{am}^{m} is the departure time for m-th bus in am. Similarly, AT_{pm}^{m} and DT_{pm}^{m} are arrival and departure times in pm.

$$\begin{aligned} AT_{am}^{m} &= random('norm', 600, 45) \\ DT_{am}^{m} &= random('norm', 990, 45) \\ AT_{pm}^{m} &= random('norm', 1380, 45) \\ DT_{pm}^{m} &= random('norm', 1440+330, 45) \end{aligned} \tag{2}$$

In the morning, *m*-th electric bus needs Tc_{am}^{m} minutes for its battery to be fully charged. In the afternoon, Tc_{pm}^{m} minutes are needed. CS100kW and CS60kW are the charging speed for 100kW and 60 kW charger respectively. The unit for charging speed is percent per minute.

$$\begin{aligned} Tc_{am}^{m} &= (1 - SoC^{m}) / CS_{100kW} \\ Tc_{pm}^{m} &= (1 - SoC^{m}) / CS_{60kW} \end{aligned} \tag{3}$$

The maximum charging time for *m*-th electric bus in day or night time is the time period between arrival and departure time. If *m*-th bus's battery is fully charged before departure, the actual charging time is Tc^m (full-charge time for *m*-th bus's battery). On the other hand, if the battery could not get fully charged before departure, the actual charging time would be $DT^m - At^m$ (time period between arrival and departure time). Therefore, the actual charging time for *m*-th electric bus is the minor value between full-charge time and maximum charging time.

$$\text{Actual charging time } = \min[Tc^m, (DT^m - AT^m)] \quad (4)$$

Other simulation requirements are

1. State of charge (SOC) ≥ 0
2. Departure time > Arrival time

Input all these parameters explained before, and run simulation three times, From Figure 1, it can be easily figured out that the contours of load curves are similar. But, there are some slight differences between each time. The daytime peak lies at around 11:00 am. The nighttime one is at about 0:00 am. Additionally, daytime peak is higher than night one by about 2400 kW.

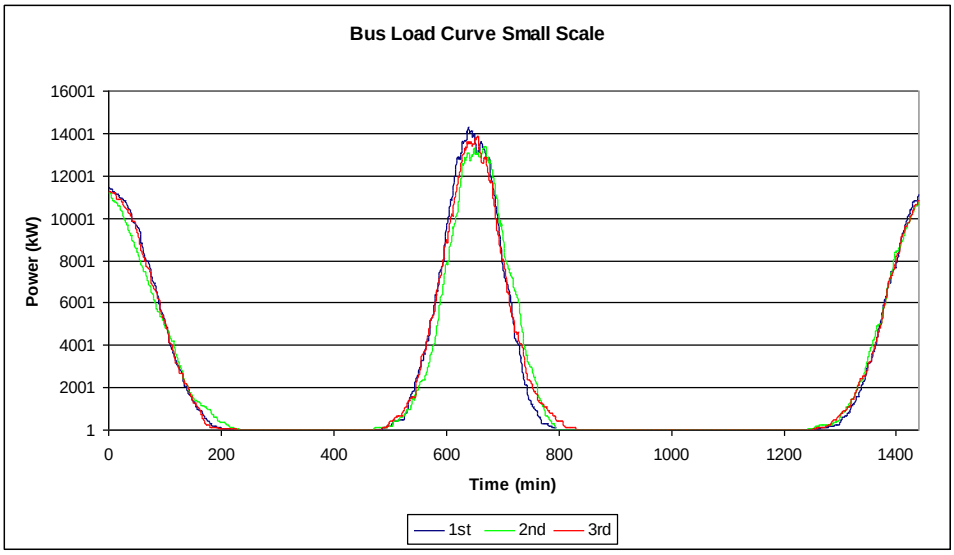

Figure 1 Three times of bus load simulation

Select one sample from these three as the result for electric bus charging load. The small-scale simulation size is 200 buses. The day time peak is 14.3 MW at 10:49 am. Daytime peak is higher than night one by 2720 kW.

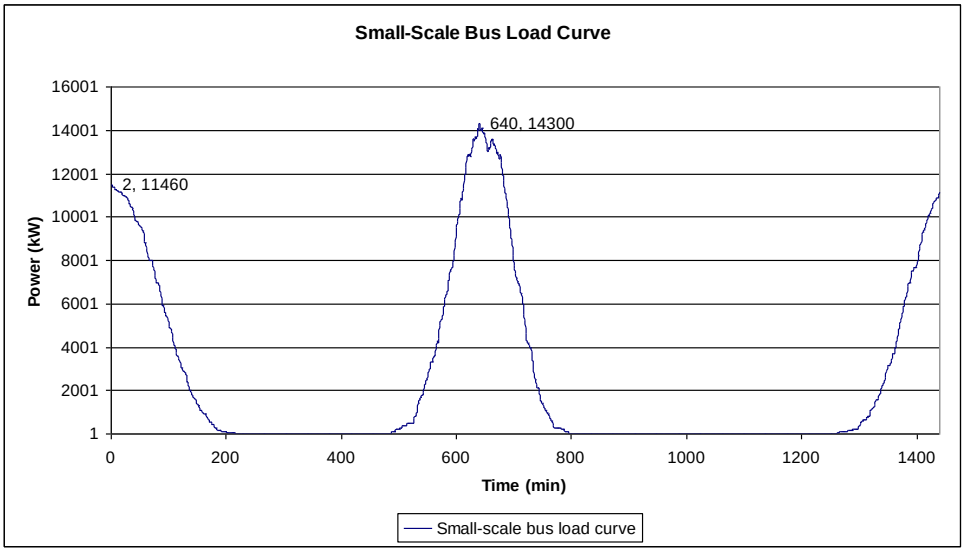

Figure 2 Small-scale electric bus load curve

Taxis are also a considerable part in urban transportation system, especially in highly-developed modern city, because parking is always the difficult problem in downtown area. Taxi become the first choice for many people if they not want to spend to much time in finding a parking lot or spend too much on parking fee.

Taxis' daily mileage is from 217 to 310 miles [13]. Operation time for most of taxis is 24 hours. But driver may change shifts. BYD e6 has been operated as taxi in Shenzhen, China, in small scale. So, it is chosen as the model of taxi. Its EDC is 186.4 miles [14]. Considering taxi's long daily mileage, two times of charging in one day is necessary. Since the difference between commuting hour and normal hour is not quite obvious for taxi drivers, they may choose to charge battery when they have lunch break or they make shifts at mid night. As a result, the first charging period is from 11:30 am to 2:00 pm. Another charging period is from 2:00 am to 4:00 am at night time when they give taxi to another driver. Charger for both time periods must be fast three-phase fast charger. Parameters for taxi charging load simulation are listed in Table 4.

Table 4 BYD e6 parameters [14]

Items	Parameters		
Dimensions & Weight	L/W/H (Unload)	4560/1822/1630 (mm)	179.5/71.7/64.2 (in.)
	F/R Overhan	920/810 (mm)	36.2/31.9 (in.)
	Wheelbase	2830 (mm)	111.3 (in.)
	Track (F/R)	1556/1558 (mm)	61.3/61.3 (in.)
	Min ground clearance	1388 (mm)	5.4 (in.)
	Min turning diameter	11 (m)	36.1 (ft)
	Curb weight	23600 (kg)	5202.9 (lb)
	Tire	225/65 R17	
Performance	Top speed	140 (km/h)	87.0 (mph)
Range	Urban range	300 (km)	186.4 (mi)
Motor	Max power	75 (kW)	100.6 (hp)
	Max torque	450 (N*m)	332.1 (ft*lb)
Suspension & Steering	Front	Dual wishbone and independent suspension	
	Rear	Dual wishbone and independent suspension	
	Steering system	EHPS	
Recharge System	BYD C100D charger & discharger	Power	100 (kW)
		Time	40 (min)
	BYD C60 DC charger	Power	60 (kW)
		Time	1.5 h
	BYD C10 DC charger	Power	10 (kW)
		Time	6 h
	On-board charger	Power	3.3 (kW)
		Time	20 h

Table 5 Taxi time schedule

Taxi		
Average daily mileage	217-310 miles	
Operation time	24 hours	
Peak periods	6:30-9:00	Commuting hour
	16:30-18:30	
Interval	N/A	
	N/A	
Mileage capacity	186 miles	
Charging times	2 times a day	Take safety factor into consideration
Charging periods	11:30-14:00	Day time
	2:00-4;00	Night time
Starting SOC	Normal distribution N (0.3, 0.1)	

Taking limited charging time and long daily mileage into consideration, the average starting SOC of taxi should be lower than that of bus and private vehicle. So, the average SOC was set to 30%.

$$\begin{aligned} SOC_{Taxi}^{m} &= random('norm', \mu, \sigma) \\ \mu_{Taxi} &= 0.3 \\ \sigma_{Taxi} &= 0.1 \end{aligned} \tag{5}$$

Arrival and departure time is defined similarly to electric bus according to Table 5.

$$AT_{am}^{m} = random('norm', 690, 30)$$
$$DT_{am}^{m} = random('norm', 840, 30)$$
$$AT_{pm}^{m} = random('norm', 120, 60) \quad (6)$$
$$DT_{pm}^{m} = random('norm', 240, 60)$$

AT_{am}^{m} , DT_{am}^{m} , AT_{pm}^{m} and DT_{pm}^{m} are all normal distribution. The time period between arrival and departure time is only about 2 hour. Consequently, Taxi drivers must use 100 kW three-phase charger in charging station. Taxi drivers have more room to choose their lunch time and shift time. So, standard deviation for AT and DT in daytime is larger than that of electric bus. The exact time that taxi drivers make shifts are mainly based on their preference. Thus, the standard deviation for AT and DT in night time is set to one hour.

$$Tc_{am}^{m} = (1 - SoC_{am}^{m}) / 0.025$$
$$Tc_{pm}^{m} = (1 - SoC_{pm}^{m}) / 0.025 \quad (7)$$

From Table 4, the fully-charge time of BYD C100D charger is 40 minutes. Therefore, the charging speed for BYD C100D charger is 2.5 percent per minute.

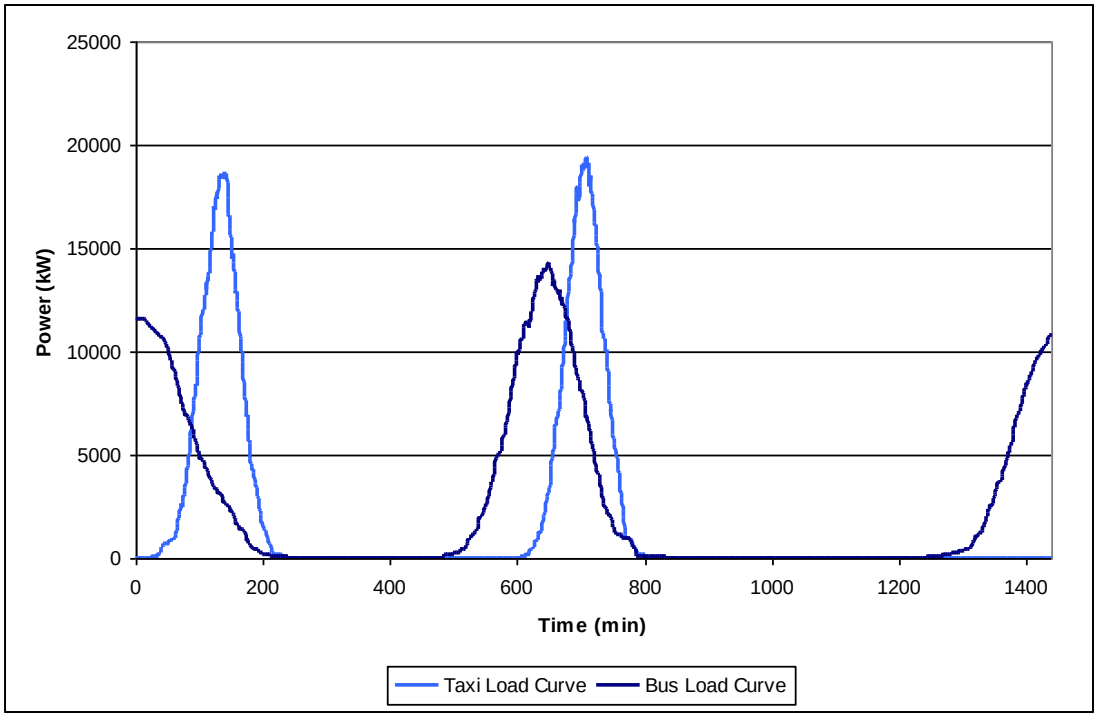

Figure 3 Taxi load curve

Compared to electric bus's curve, loads are concentrated at 2:30 and 11:00. The peak load is 19.4 MW. Taxi is the only type of vehicle that charge batteries in a large scale at night. If real-time pricing is put into practice, commonly, the price is comparatively low at midnight due to low total demand. So, taxi drivers may have strong incentive to charge at midnight. And, this peak load would not have a significant effect on the grid.

◆ Private vehicle charging pattern

Average daily mileage for private car is only about 42 miles a day. The mileage is much fewer than that of bus and taxi. BYD e6 is still chosen as the model of main stream

sedan. Take safety factor into consideration, owner of PHEV should charge battery every two days at home or in workplace.

Private vehicle's main function is commuting. So, charging periods starts when they arrive at working place or arrive home. The first charging period lies between 7:30 and 17:00. The second period begins at 19:00 and ends at 7:00. It can be easily figured out that charging time for private car is comparatively abundant. Therefore, for both periods, slow charging mode is the first option. 100 kW fast charging mode is only for long distance travelling or emergency.

In United States, the ratio for sedan and SUV is about 6:4. SUV also accounts for a considerable share in private vehicles. BYD S6DM is selected as the model for SUV. In consideration of output power and mileage capacity, S6DM is designed as a dual mode hybrid vehicle, not pure electric one. Detailed parameter is shown in below table.

Table 6 S6DM Hybrid SUV parameters [14]

Items	Parameters		
Dimensions & Weight	L/W/H (Unload)	4810/1855/1725 (mm)	189.4/73.0/67.9 (in.)
	Wheelbase	2715 (mm)	106.9 (in.)
	Fuel tank capacity	45 (L)	11.9 (gal.)
	Tire	225/65 R17	
Performance	Top speed	>= 180 (km/h)	>= 111.8 (mph)
Range	EV Range	>= 60 (km)	>= 38.0 (mi)
Motor	Motor type	Permanent-magnet type synchronous motor	
	Max power	85 (kW)	114.0 (hp)
	Max torque	450 (N*m)	332.0 (ft*lb)
Engine	Engine model	BYD483QB	
	Displacement	1.998 (L)	
	Max power	103 (kW)	138.1 (hp)
	Max torque	186 (N*m)	137.2 (ft*lb)
Suspension & Steering	Front	McPherson strut type	
	Rear	McPherson strut type	
	Steering system	EPS	
Recharge System	Home charge	Power	2 (kW)
		Time	8 h

$$\begin{aligned} SOC_{PV}^{m} &= random('norm', \mu, \sigma) \\ \mu_{PV} &= 0.5 \\ \sigma_{PV} &= 0.1 \end{aligned} \tag{8}$$

SOC_{PV}^{m} is the starting SOC of *m*-th private vehicle. Mean value is 50% and standard deviation is 10%. Owners of PHEVs are suggested not to deeply charge their batteries.

Parameters about time schedule for private vehicles in daily commuting is summarized in Table 7.

Table 7 Private vehicle time schedule

Private car		
Average daily mileage	42 miles	
Operation time	Commuting hour	
Peak periods	6:30-9:00	Commuting hour
	16:30-18:30	
Interval	N/A	
	N/A	
Mileage capacity	190 miles	
Charging times	every two days	Take safety factor into consideration
Charging periods	7:30-17:00	Day time
	19:00-7:00	Night time
Starting SOC	Normal distribution N (0.5, 0.1)	

$$\begin{aligned} AT_{am}^{m} &= random('norm', 450, 45) \\ DT_{am}^{m} &= random('norm', 1020, 45) \\ AT_{pm}^{m} &= random('norm', 1140, 60) \\ DT_{pm}^{m} &= random('norm', 420, 60) \end{aligned} \tag{9}$$

The charging periods for private vehicle are after commuting hours. The arrival and departure time is set according to Table 7 in normal distribution.

Sedan

$$Tc_{am}^{m} = (1 - SoC_{am}^{m}) / 0.00278$$

$$Tc_{pm}^{m} = (1 - SoC_{pm}^{m}) / 0.00278$$

SUV (10)

$$Tc_{am}^{m} = (1 - SoC_{am}^{m}) / 0.00208$$

$$Tc_{pm}^{m} = (1 - SoC_{pm}^{m}) / 0.00208$$

In both charging periods, the owners of PHEVs charge their vehicles in workplace or at home. So, C10D, 10 kW charger, is suitable for compact sedan owners. The fully-charge time is 6 hour. 2kW charger is selected for SUV owners. Both charging speeds are adapted to percent per minute in Equation (10).

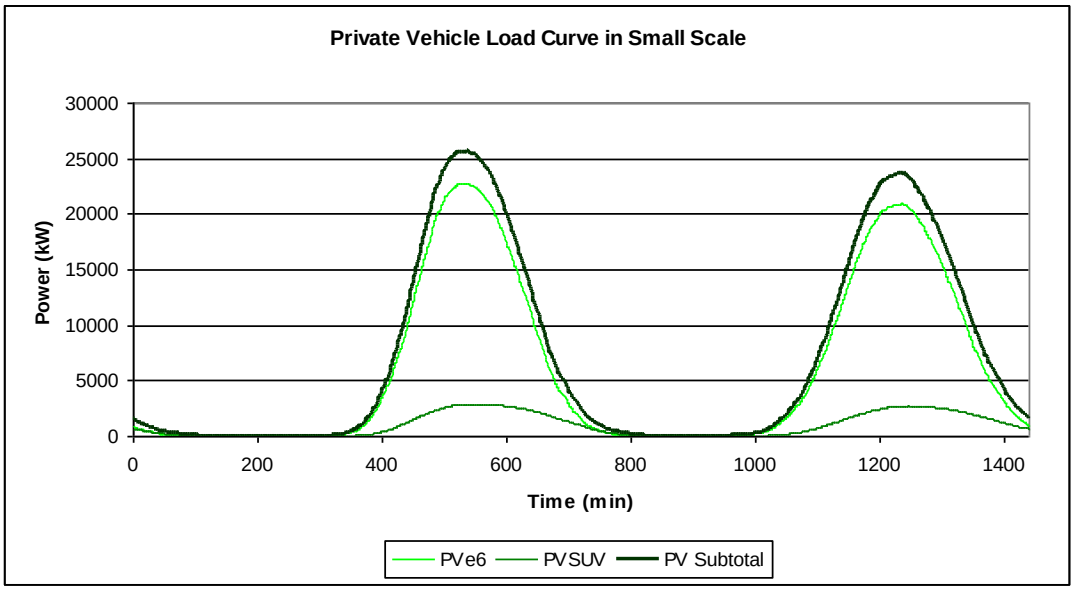

Figure 4 Private vehicle load curve in small scale

Similar to the curves of bus and taxi, load peak still appears at noon. So, the highest peak at noon for all PHEVs could be expected. Due to long fully-charge time, loads for private vehicle allocates more evenly.

◆ Charging pattern for all types of PHEVs

Next step, loads for all types of PHEVs are summarized in one chart

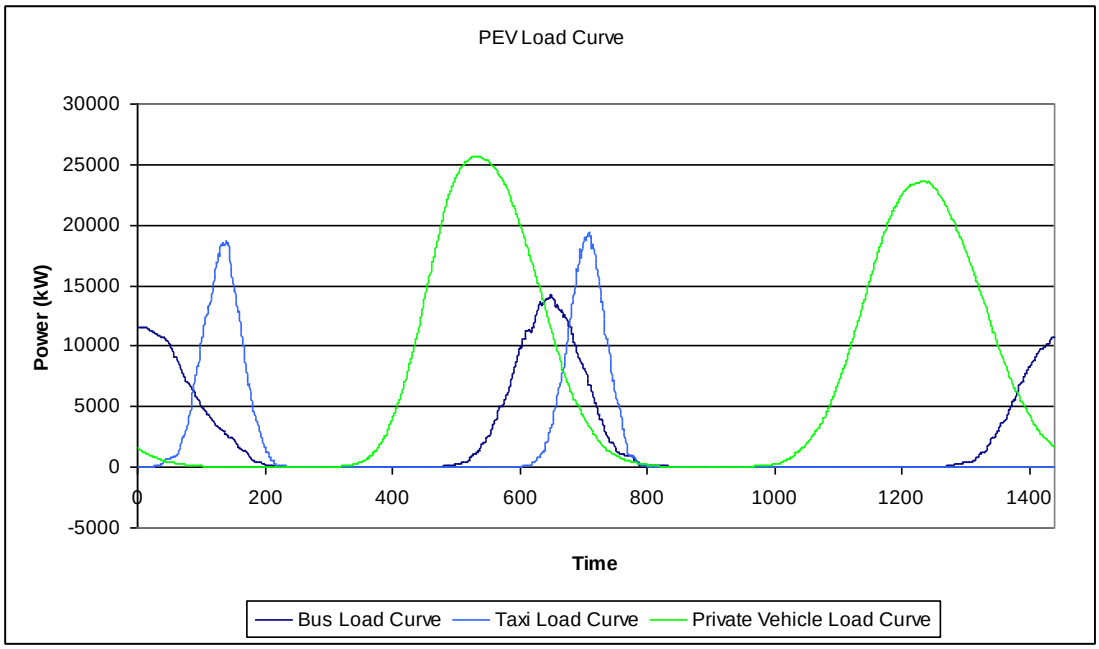

Figure 5 PHEV load curve separately

From Figure 5, loads of private vehicle take the largest part of all types of electric vehicles. Its load peak appears at 8:59 and its value is about 25.7 MW. Load peaks for bus and taxi show up later at noon. Public bus' charging peak locates at 10:49 and its value is 14.3 MW. The latest load peak is taxis'. It appears at 11:50 and its values is 19.4 MW. In

night time, three load peaks for three types of vehicles arise separately. They are at 20:36, 0:05 and 2:20.

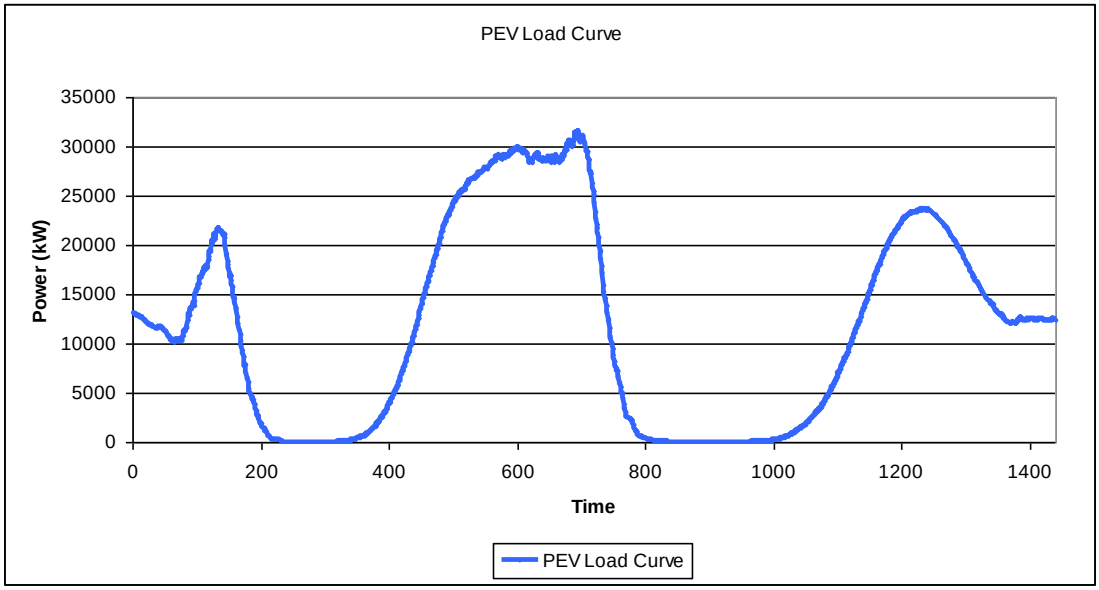

Figure 6 Subtotal PHEV load curve

In small-scale simulation (Bus: 200; Taxi: 500; Private sedan: 10000; Private SUV: 6000), If load curves for all three types of PHEVs are added together, the load peak is at 11:35 a.m. The peak value is about 31.6 MW. Load grows continuously before the peak and drops suddenly after peak. That means there is a lot of potential to shift the peak backwards to relief the pressure to grid.

Since three loads peaks arise in the morning one by one, the total load is at high level from 8:30 to 11:30. But, after the peak, load curve drops suddenly. Most vehicles

have finished charging after noon. That means there is a great potential to shift loads from morning to afternoon to relief the pressure to the grid.

It should also be mentioned that at commuting hour, loads in the grid is extremely low. We may suggest drivers to charge their vehicles if they do not use them at rush hour.

3.2 Charging Load Prediction in Large Scale

To analyze the impact of large-scale PHEVs, firstly, the amount of each type of PEVs in next two decades should be predicted. The annual growth rate for public bus and taxi is assumed to be 40% between 2017 and 2020 due to government subsidy. The average growth rate is reduced to 20% afterwards.

As to private vehicles, the growth rate would be evenly distributed in next two decades. Although electric vehicles saves a lot in gasoline consumption, owners of private vehicles might not change their car immediately due to high price of PHEV and worry about lack of charging station. So, this replacement of elder combustion engine vehicles would be continuous.

PHEV might have a bright future. But, the beginning for PHEV seems not smooth. Pike Research, the Colorado-based clean tech analyst firm issued its latest forecast for electric vehicles. According to this forecast, the United States will fall behind

of President Obama's widely publicized goal of having one million plug-in vehicles on American roads by 2015 [15].

Pike forecasts the number for cumulative sales of plug-in hybrid electric vehicles will be only 667,000 by 2015. But the good news is that the annual sales of PHEVs in 2016 will be 289,000, and will reach 303,000 by 2017. Referring to Pike's forecast, the U.S. will reach one million by 2017.

EV sales do not grow rapidly in US. The most critical reason is that many electric vehicle launches are delayed. Referring to delayed introductions from Ford, Mitsubishi, Coda and Fisker, their new models of plug-in electric vehicles are all postponed to next year. As a result, there are only two models available in the market. They are Nissan Leaf and Chevy Volt. Other models, such as Fisker Karma and Ford Focus Electric may arrive, but the production would not be high. So, low sales of PHEV is mainly due to supply side not demand side.

On the other hand, the market may face a new turn in 2013, many new manufacturers will join the electric vehicle market, For instance, Volkswagen, BMW and Hyundai will start selling plug-in electric vehicles. In addition, Toyota and Honda have potential to make impact on the market in future.

Even by 2017, Pike Research's report "Electric Vehicle Market Forecasts" acclaimed that pure electric car represents mere 0.8% of the U.S. market, while plug-in hybrids will account for 1.2%.

Continued supply shortages and the high price of many models Vehicles like the $57,000-plus Tesla Model S are the two main reasons for low market share. However, we still have confidence in sales of plug-in hybrids. If PHEV equips smaller batteries, that means lower cost. As mentioned before, Toyota would be that sleeping giant. Owners of the gas powered Prius is about one million. If the Prius Plug-in Hybrid can meet the expectations from customers in quality and price aspects, owners may convert to Plug-in Hybrid in a large number.

After ten years, conventional hybrids represent about 2% of auto sales. In contrast, plug-in hybrids would reach that market share in seven years. And the growth would be even faster in next ten years. Referring to the US Bureau of Transit Statistics for 2004, there are 243,023,485 registered passenger vehicles in the United States. About 136 million of them were normal 2-axle, 4-tire vehicles, such as sedan and compact car. They accounted for 56.13% share of total amount. 91 million (37.79%) were other 2-axle, 4-tire vehicles. For example, SUVs and buses are included in this type.

Not every registered vehicle is still on road. Many of them are just sitting idle or waiting for total loss. So, there are approximately 250 million vehicles on road in 2012.

About 16 million brand new cars are sold annually. Considering old cars are also scraped annually, the number of all types of vehicles in 2017 would be about 320 million. In contrast, mere one million PHEVs will on the road. However, if the amount of PHEVs increases at this rate continuously, PHEVs will account for more and more share in the market. The detailed amount for each type of electric vehicle is listed in Table 8.

Table 8 Amount of PHEV in 2017, 2020 and 2030 [16]

Amount of Plug-in Electric Vehicles (million)					
	Public bus	Taxi	Sedan	SUV	Total amount
2017	0.017	0.04	0.718	0.484	1.259
2020	0.047	0.11	1.97	1.328	3.455
2030	0.291	0.68	27.158	18.308	46.437

The annual growth rate for public bus and taxi is assumed to be 40% between 2017 and 2020. From 2020 to 2030, the average growth rate is reduced to 20%. As to private vehicles, the growth rate is more evenly distributed in next two decades.

For large-scale of PEVs, Matlab code should also be updated since iteration statement's efficiency decrease rapidly as number of vehicles is up to million level. Two loops are included in small-scale simulation model. As a result, Monte Carlo simulation method is introduced to save compute time. To further save compute time, time step is increased from 1 min to 10 min.

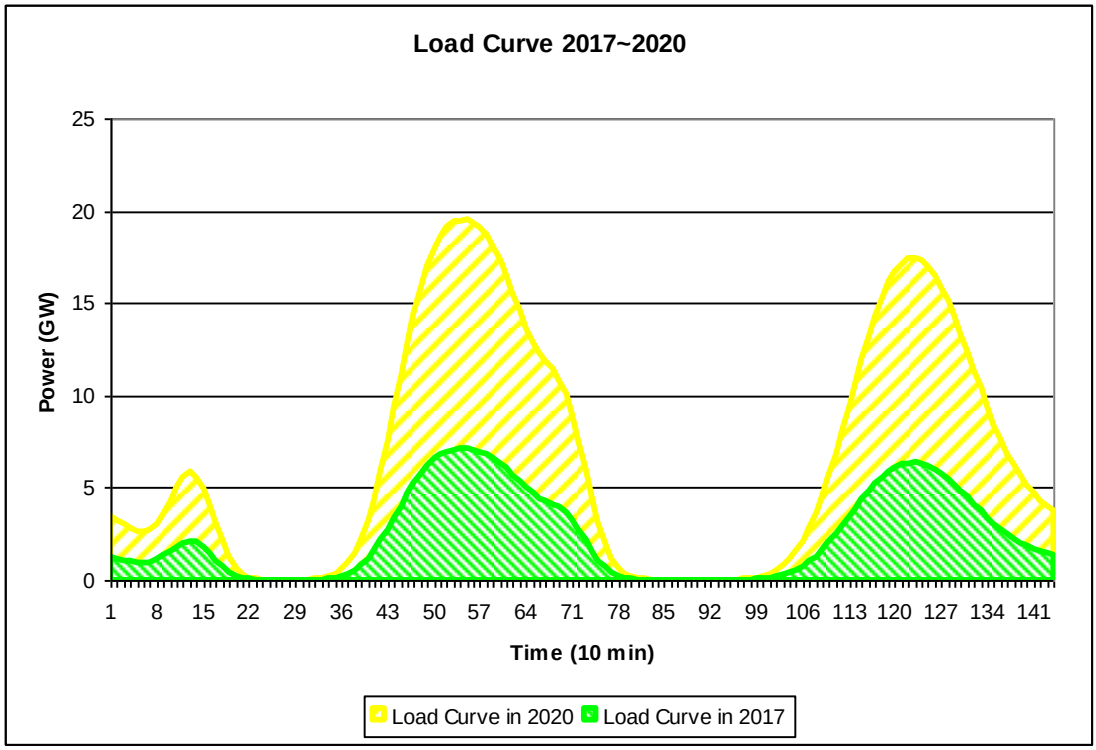

Figure 7 Load curve prediction in 2017 and 2020

In 2017, the peak at noon is expected to be 7.12 GW. In United States, the total installed capacity nationwide is about 1000 GW. Peak loads of PEVs won't have huge effect on the grid in 2017. However, this peak grows really fast. After 3 years, in 2020, it is already 19.49 GW. The load is almost tripled. Besides, two load peaks become more prominent.

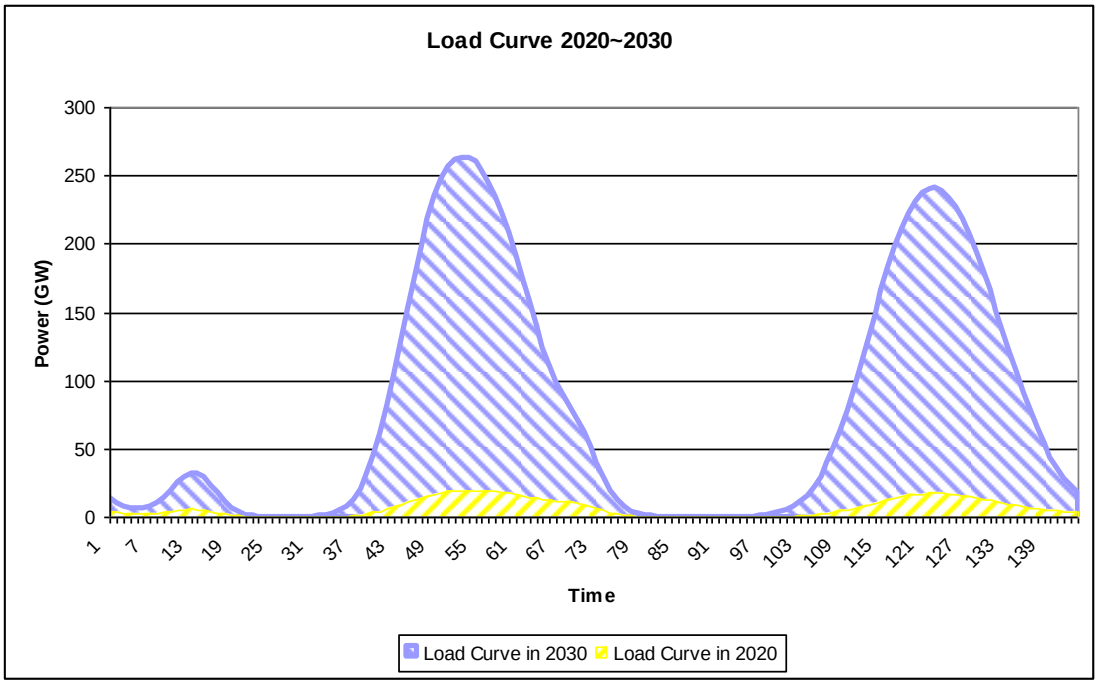

Figure 8 Load curve prediction in 2020 and 2030

After 10 years of development, PEVs would take 30% share of all kinds of vehicles. That also means its charging load become a considerable part on the grid. Its peak at noon would be 263.56 GW. Compared to load curve in 2020, loads in the evening and morning after commuting hour increase evidently. That means loads from private vehicle become more and more important. In contrast, load peak in mid night become less significant.

Chapter 4. Optimization in Regular Distribution Network

4.1 Charging Load Forecast in Regular Distribution Network

Simulation charging load data for private electric vehicles is shown in Fig 1. In the small-scale simulation, 5 Chevy Volt hybrid electric vehicles are included. In this case, it is assumed that the electric vehicle start charging battery when it is connected into the grid. If 5 PHEVs simply apply fast charging, there would be load peak at 18:00. The peak value is 19.2 kW. This definitely would be a huge pressure for a 25-kVA distribution transformer. Compared to fast charging option, if normal or slow charging option is applied. The charging load curve would be much smoother. The peak load value of normal charging option is 7.2 kW. The peak load value of slow charging option is even lower. It is only 4.8 kW. The relationship between extra charging loads and aging of transformer would be explained in following section.

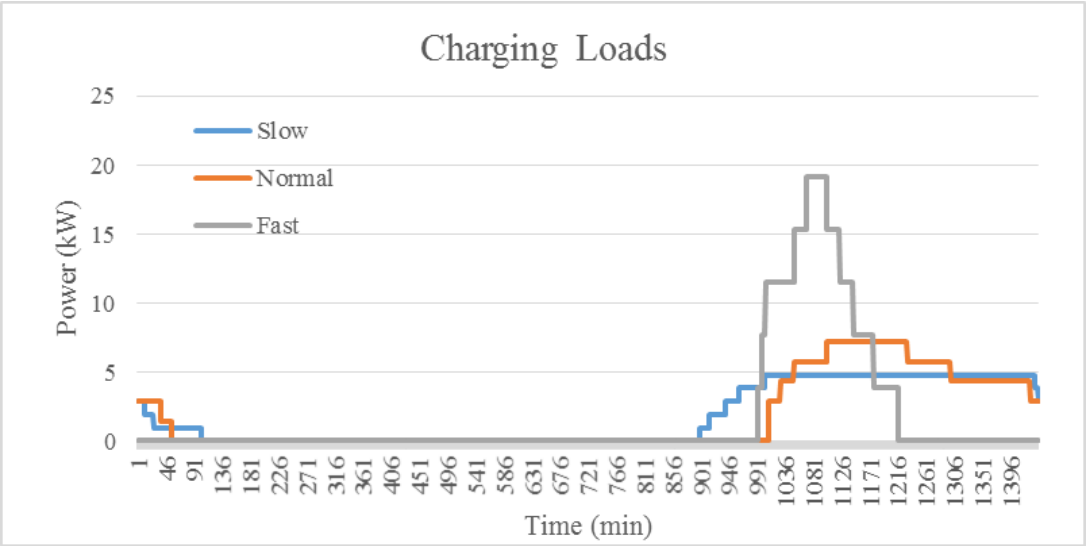

Figure 9 Plug-in electric vehicles load curves of three charging options

4.2 Charging Load Schedule Optimization for Distribution Transformer

In regular distribution network, the first electric appliance that can be greatly affected by PHEVs' charging load is distribution transformer. Transformer's relative loss-of-life is mainly related to the LV/HV wiring insulation. The insulation is in the function of hot-spot temperature. In this dissertation, hot-spot temperature is calculated using the IEEE method. This method applies to oil-filled transformers. The equation is given below. This method applies to oil-filled transformers.

$$\theta_H = \theta_A + \Delta\theta_{TO} + \Delta\theta_H \quad (11)$$

Where

θ_A = ambient temperature

$\Delta\theta_{TO}$ = temperature gradient of the top oil temperature over the ambient temperature

$\Delta\theta_H$ = temperature gradient of the hot spot over the top oil temperature

If loads changes, $\Delta\theta_{TO}$ and $\Delta\theta_H$ are given by following equations

$$\Delta\theta_{TO} = (\Delta\theta_{TO,U} - \Delta\theta_{TO,i})(1 - e^{-t/\tau TO}) + \Delta\theta_{TO,i} \quad (12)$$

Where

$\Delta\theta_{TO,U}$ = ultimate steady-state top oil temperature gradient

$\Delta\theta_{TO,i}$ = initial top oil temperature gradient

t = duration of the load change, h

τ_{TO} = oil time constant, h

$$\Delta\theta_{TO,i} = \Delta\theta_{TO,R}\left(\frac{K_i^2 R + 1}{R + 1}\right)^n \quad (13)$$

Where

R = ratio of load losses at rated load to no-load losses from the test report

K_i = ratio of the initial load to the rated load

$\Delta\theta_{TO,R}$ = top oil temperature gradient at rated load from the test report

n = an empirical exponent that depends on the cooling class

$$\Delta\theta_{TO,U} = \Delta\theta_{TO,R}\left(\frac{K_U^2 R+1}{R+1}\right)^n \quad (14)$$

Where K_U = the ratio of the ultimate (final) load to the rated load

The winding hot temperature gradient is given by

$$\Delta\theta_H = (\Delta\theta_{H,U} - \Delta\theta_{H,i})(1-e^{-t/\tau W}) + \Delta\theta_{H,i} \quad (15)$$

Where

$\Delta\theta_{H,U}$ = ultimate steady-state hot-spot temperature gradient

$\Delta\theta_{H,i}$ = initial hot spot temperature gradient

τ_W = winding time constant, h

$$\Delta\theta_{H,i} = \Delta\theta_{H,R} \times K_i^{2m}$$
$$\Delta\theta_{H,U} = \Delta\theta_{H,R} \times K_U^{2m} \quad (16)$$

Where

$\Delta\theta_{H,R}$ = the hot-spot temperature gradient at rated load from the test report

m = an empirical exponent depending on the cooling class

The aging acceleration factor (F_{AA}) is the ratio of the per unit life at the design temperature of 100°C divided by the per unit life at some operating temperature θ_H .

$$F_{AA} = e^{39.16 - 15000/(\theta_H + 273)} \quad (17)$$

The equivalent aging of a transformer, F_{EQA}, can be obtained by averaging the F_{AA} over the period of time that the transformer is under study.

$$F_{EQA} = \frac{\sum_{n=1}^{N} F_{AA,n} \Delta t_n}{\sum_{n=1}^{N} \Delta t_n} \quad (18)$$

The hours of life lost in the total time period is

$$T_{Loss} = 24 * F_{EQA} \quad (19)$$

Percent loss of life (LOL%) in the time period is

$$LOL\% = \frac{T_{Loss}}{1.8e5} \times 100\% \quad (20)$$

If no EV charging load is added, the aging acceleration factor versus time in condition of base loads is shown in Figure 10. All necessary parameters of 25-kVA distribution transformer is available in [17]. Base load curve data is from RELOAD database [18].

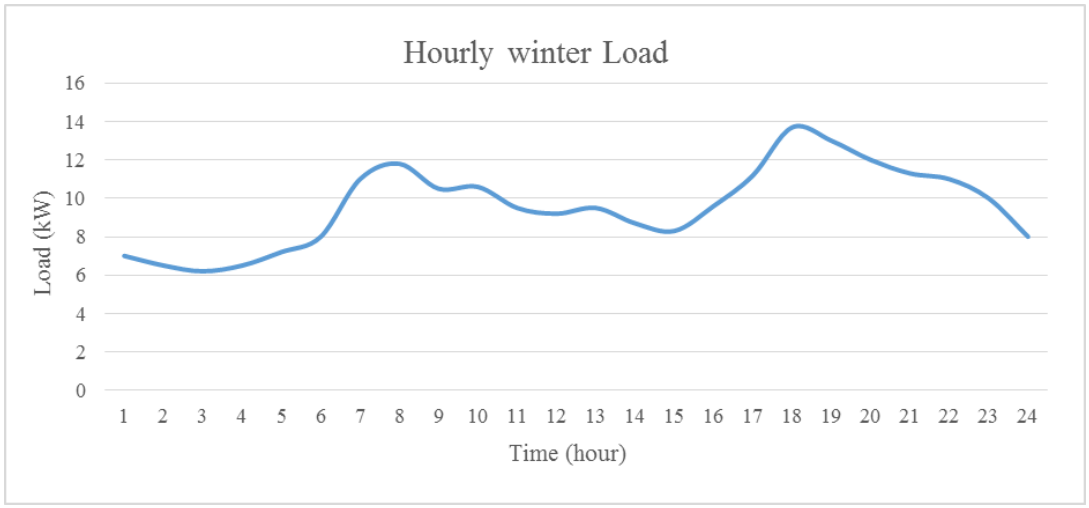

Figure 10 Hourly winter load seen by a 25 kVA transformer

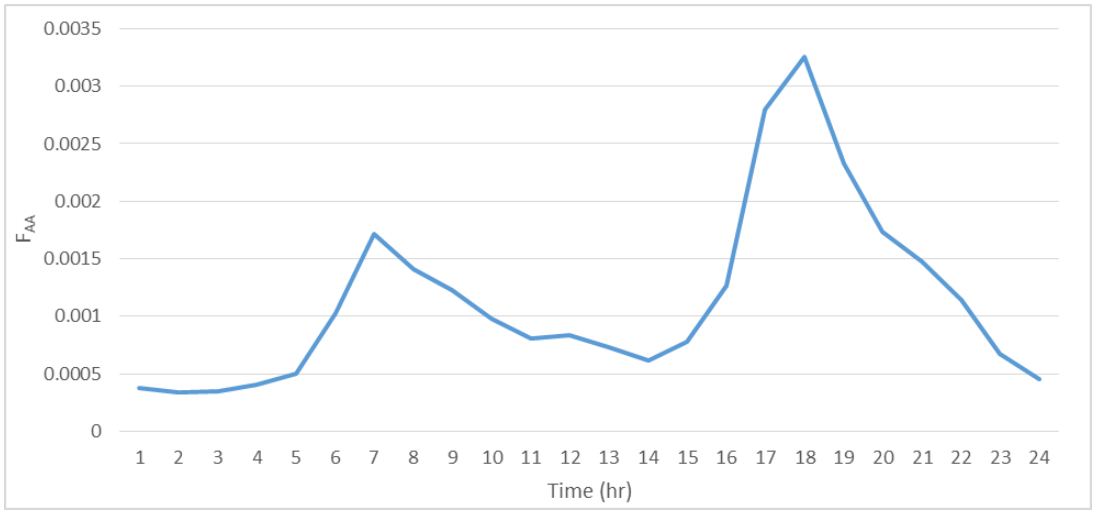

Figure 11 F_{AA} curve in base loads condition

◆ PHEV charging schedule optimization for distribution transformers

In simulation conducted in previous sections, owners of PHEVs start charging their vehicles when batteries are plugged into the grid. There is great potential to re-coordinate

the charging scheme, so as to relieve its impact on the distribution transformer. Since the available charging time for private vehicles is abundant. There is great potential to shift peak loads backwards, and then relief the pressure on transformer and improve the aging program due to extra battery charging loads. Obviously fast charging has the greatest impact on transformer aging. The F_{AA} curve in condition of 5 fast-charging PHEVs is shown in Figure 12.

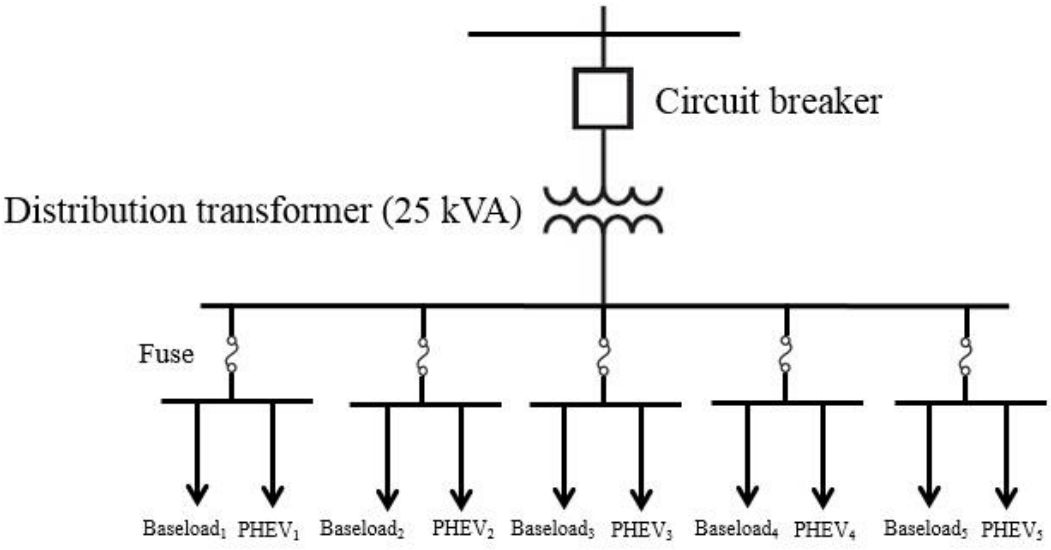

Figure 12 25-kVA distribution transformer network

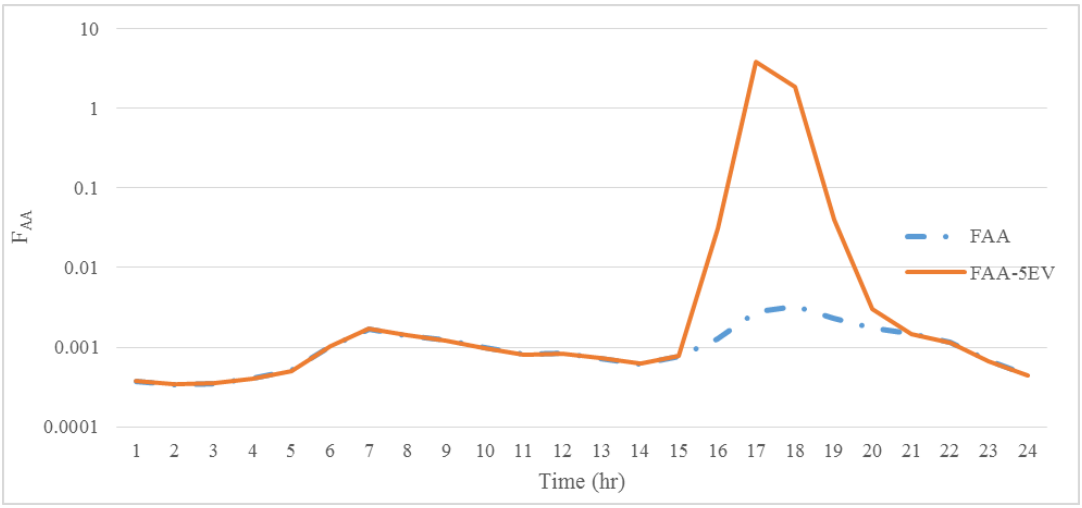

Figure 13 F_{AA} curve in condition of 5 fast-charging PHEVs

Particle swarm optimization method is introduced to find the best start charging time for each vehicle. Particle swarm optimization utilize Pseudo velocity – magnitude a function of distance from minimum which is given in below equation. Main objective function is shown in the following equation.

$$V_{k+1}^{i} = W_k V_k^{i} + c_1 r_1 (p_k^{i} - x_k^{i}) + c_2 r_2 (g_k - x_k^{i}) \quad (21)$$

Where

p_k^{i} = best location for particle i up to time k

g_k = global best location up to time k

r_1 and r_2 = random numbers [0, 1]

c_1 and c_2 = cognitive and social scaling parameters

W_k = initially 1 and gradually reduced

Particles are initially randomly distributed through design space, $x_{lb} \le x_0^i \le x_{ub}$.

Velocities are initialized randomly from $0 \le V_0^i \le V_0^{\max}$. $V_0^{\max} = 0.5(x_{ub} - x_{lb})$.

Main objective function is shown in the following equation.

$$\min \quad F_{EQA} = \frac{\sum_{n=1}^{N} F_{AA,n} \Delta t_n}{\sum_{n=1}^{N} \Delta t_n} \quad (22)$$

Constraints are as follows.

$$X_m \ge At_m$$
$$0.2 \le SOC_m \le 1 \quad (23)$$

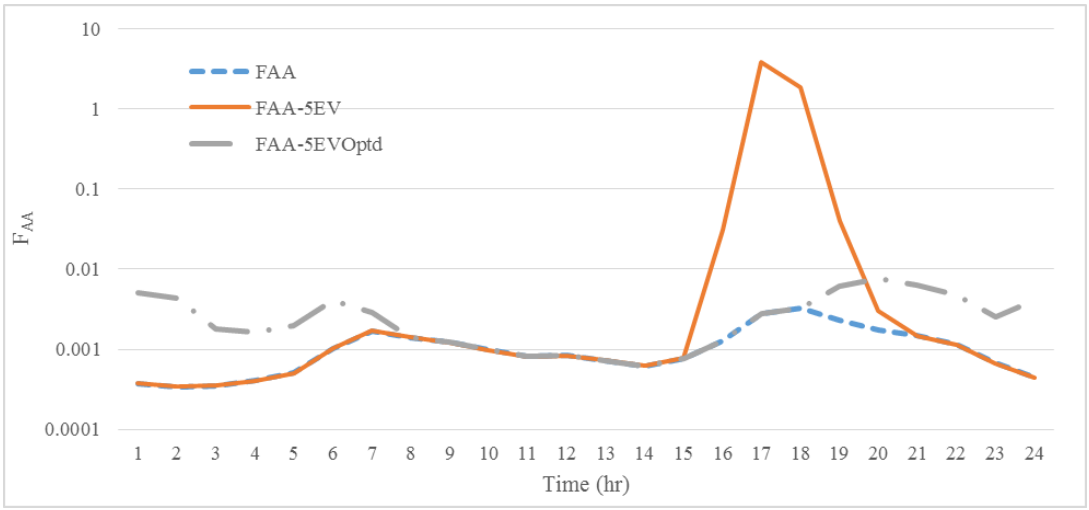

Figure 14 F_{AA} with 5 PHEV after optimization

Table 9 Comparison of loss of life after optimization

	F_{EQA}	LOL%
BaseLoad	2.720E-02	1.511E-05
Extra 5 EVs	5.792E+00	3.218E-03
Extra 5 Evs after optimization	6.787E-02	3.771E-05

From

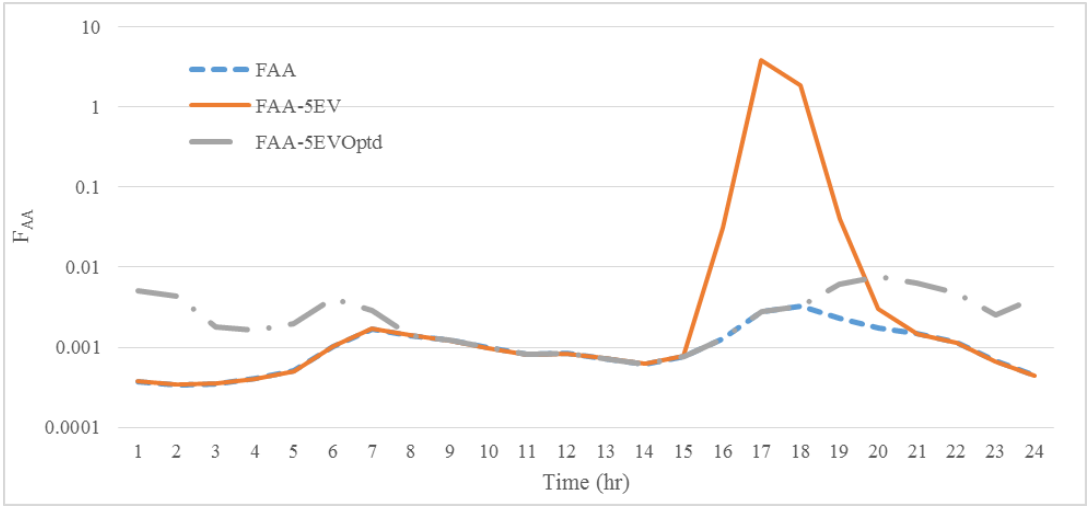

Figure 14, the FAA curve is clearly smoothed out after optimization. The peak FAA value is successfully reduced from 3.84 to 7.6e-3. From Table 9, F_{EQA} and LOL% also decrease evidently after charging time re-scheduling. The loss-of-life over 24-hour is decreased by 98.82% percent. The particle swarm optimization method helps to improve distribution transformer aging problem effectively without interfere individual PHEV owner's charging habit.

4.3 V2H and Demand Response System Theory

In the following section, based on the charging schedule generated from V1G method, each private vehicle is assigned a better starting charging time. Then, the Vehicle to Home (V2H) charging method is applied to organize the daily charging schedule of PHEVs for each house. The battery of PHEV serves as an energy storage device. The objective is to develop an integrated charging scheme based on the real-time subtotal household loads to avoid exceeding demand limit for each house. The vehicle battery may supply or absorb the electricity to home depending on its battery SOC. The charging/discharging strategy is Figure 15 [13].

Figure 15 V1H strategy considering different SOC level

In Figure 15, SOC1 is the first level of battery charging. Under this level, the battery needs to charge. Once the charging process starts, the system is not able to shut it down until battery SOC reaches SOC1. SOC2 is the second level. If the battery SOC is above this level, PHEV is ready to participate in V2H system and supply power back to the house.

Demand response is included in V2H system as well. Loads in each house could be defined into two categories, unresponsive loads (Lu) and responsive loads (Lr). Energy management system may shut down certain controllable load depending on load priority setting of each house if the subtotal load is over the demand limit (DL). The

demand limit level could be flexible or flat rate. In this dissertation, flat rate demand limit is applied. Once this demand limit level is set, the HAN control center will perform V2H in real time to each house according to the load priority and preference setting individually. Each electric appliance has a Rank value. Rank = 0 means that the appliance is critical or uncontrollable. The higher rank value means the less important in consumer's setting. For instance, if the subtotal load (Ls) is over the demand limit and if the water heater is ON and has the highest rank value, DR would turn off the water heater first and check whether Ls is still over DL. If the load value is below the limit, all controllable loads will resume their normal operation. If not, DR may find the second less important controllable load to turn off.

- Single deterministic model testing

The flat demand limit is set as 6.5 kW. Then V2H strategy is performed according to the rank setting in Table 10 and the V2H strategy shown in Figure 16. Since BYE e6 is pure electric vehicle and it is not practical in United States yet, Chevy Volt is chosen as the PHEV model instead to test V2H method. Chevy Volt has three charging options: slow, normal and fast. To test the extreme condition, fast charging is chosen since it needs the most power. All charging options and full-charge time are shown in Table 11.

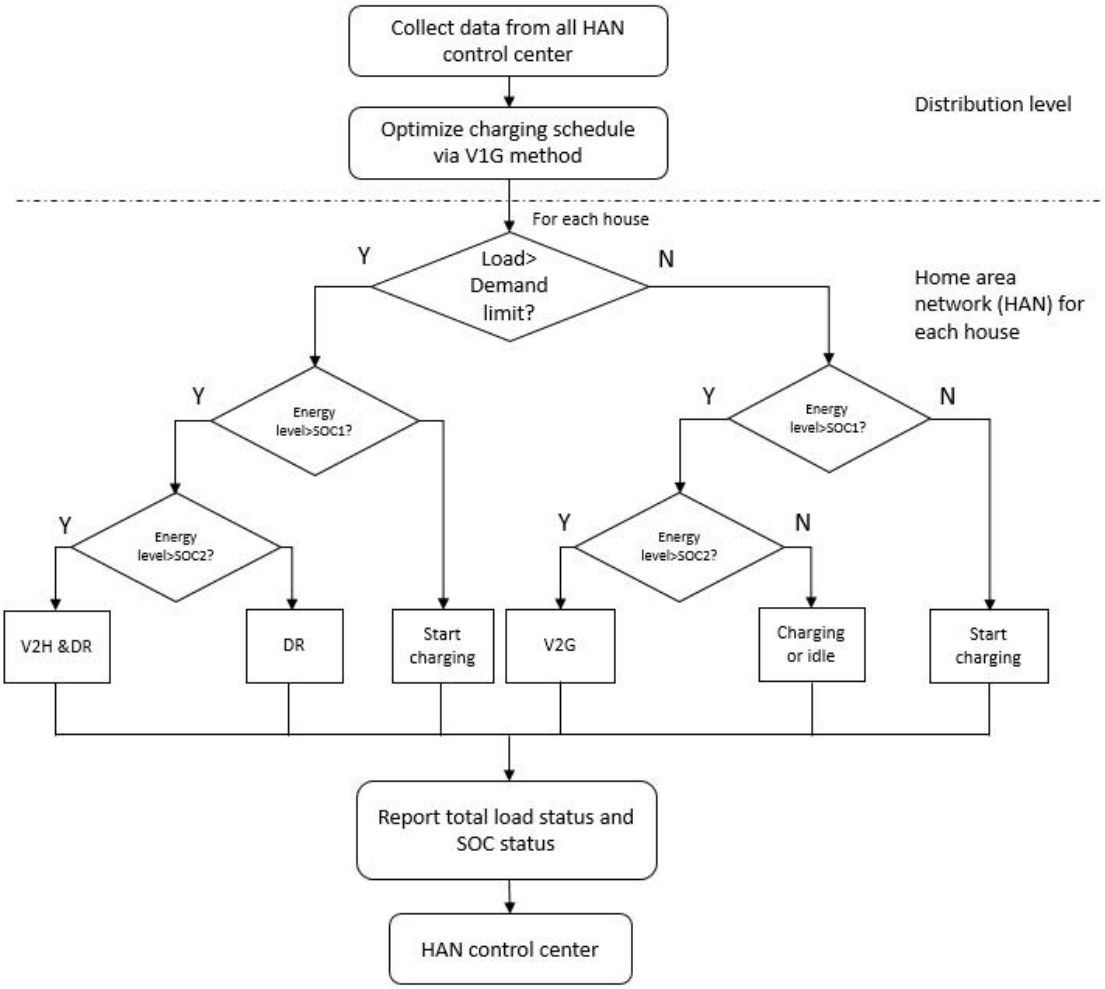

Figure 16 Flow chart of V1G and V2H system

Table 10 Rank setting

Index	**Appliance**	**Power (kW)**	**Status (S_i)**	**Rank (R_i)**
1	Refrigerator	0.5	1~24	0
2	Water heater	5	1, 16	2
3	Air conditioner	2	1, 2, 8~24	3
4	Washer & Clothes dryer	2	17, 18	4
5	Electric vehicle	3.84 (Fast charging)	17, 18, 19	1

Table 11 Chevy Volt charging options

Charging Circuit	Charge Power (kW)	Charge Duration (hour)
Slow Charge (120V/8A)	0.96	8.3
Normal Charge (120V/12A)	1.44	5.6
Fast Charge (240V/16A)	3.84	2.1

From Figure 17, it is clear that with the V2H method the load curve is evidently smoothed out. PHEV is plugged in at 16:00. Without V2H strategy, the subtotal load would be above the demand limit at 16:00, 17:00 and 18:00. Furthermore, the peak value is 11.34 kW at 16:00. This peak value is almost twice the demand limit. If the V2H method applied to this case, loads of charging PHEV are shifted backwards to avoid creating a load peak. The actual charging period is from 19:00 to 23:00. In the meantime, the subtotal load is controlled under a flat demand limit (6.5 kW) successfully.

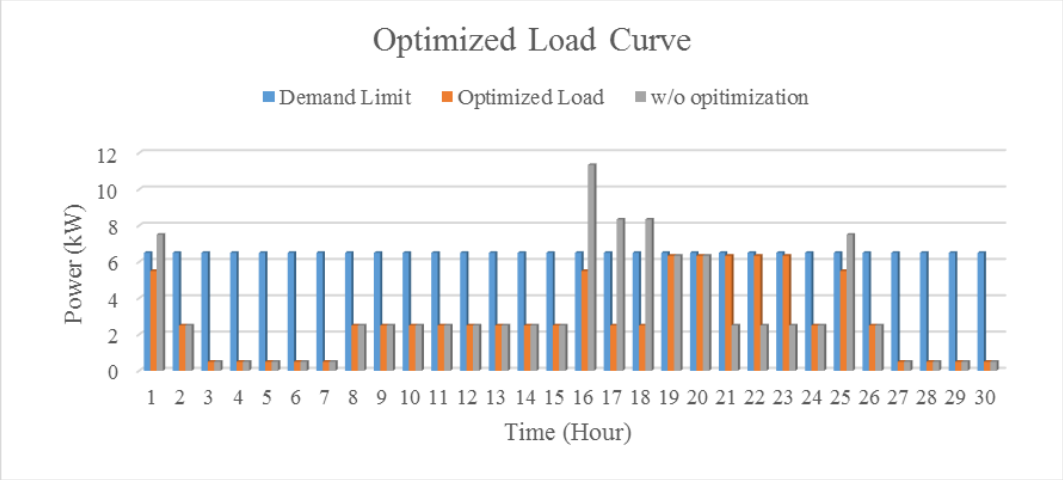

Figure 17 Optimized load curve under low-SOC condition

(Plug-in SOC = 0.2)

Chapter 5. Optimization in Microgrid

5.1 Renewable Energy Sources Modelling

Solar and wind are two main stream micro power sources that are widely used in microgrid. Compared to traditional power plant, they both cannot provide a stable output. It is hard to forecast the outputs from both renewable energy sources. Consequently, the economic dispatch for all power sources in microgrid is difficult to be performed due to the uncertainties induced by renewable energy sources.

The fluctuation of wind farm power output is due to the continuous change of wind speed. Similarly, the output of solar farm is dependent on radiation from sun. In daytime, the solar altitude angle and insolation changes seasonally. In this dissertation, a versatile probability distribution model is used to represent the forecast error for both renewable sources in microgrid and applied to economic dispatch problem.

To begin with, the probability density function (PDF), cumulative distribution function (CDF), and inverse function of CDF of versatile distribution are shown below [19].

$$f(x|\alpha,\beta,\gamma)=\frac{\alpha\beta e^{-\alpha(x-\gamma)}}{(1+e^{-\alpha(x-\gamma)})^{\beta+1}} \quad (24)$$

$$F(x|\alpha,\beta,\gamma)=(1+e^{-\alpha(x-\gamma)})^{-\beta} \quad (25)$$

$$F^{-1}(c|\alpha,\beta,\gamma)=\gamma-\frac{1}{\alpha}\ln(Cs^{-1/\beta}-1) \quad (26)$$

where

x: random variable

$\alpha,\ \beta,\ \gamma$: shape parameters

Cs: confidence level

The reasons why versatile distribution is a better option to represent the forecast error of renewable energy sources' outputs are

1. Suitable values for shape parameters can be determined from historical data. The root-mean-square error (RMSE) between actual CDF and versatile CDF is much smaller than the RMSE between actual CDF and Gaussian/Beta CD [19].
2. The analytic forms for both CDF and inverse CDF are available for versatile distribution. This characteristic can facilitate the solution of economic dispatch problem. It will be further explained in later sections [20].

As an example, data from solar farms [21] in February is used here. The feasible output time period is from 7 a.m. to 7 p.m. daily. Outside this period, the output is almost zero due to low solar radiation. The forecast span is set as 15 days. Specifically, 15-day actual output data from a 100 kW solar farm from Feb 1st to Feb 15th is utilized to generate suitable shape parameters for versatile distribution model. The detailed procedure is explained in following section.

1. The actual CDF is generated from 15-day solar farm data;
2. 10-20 characteristic points are selected from actual CDF;
3. nlinfit/lsqcurvefit functions in Matlab are used for curve fitting according to the characteristic points.

The curve fitting results are shown in Figure 18 to compare the performance by two different functions. Power base is set as 100 kW in this dissertation.

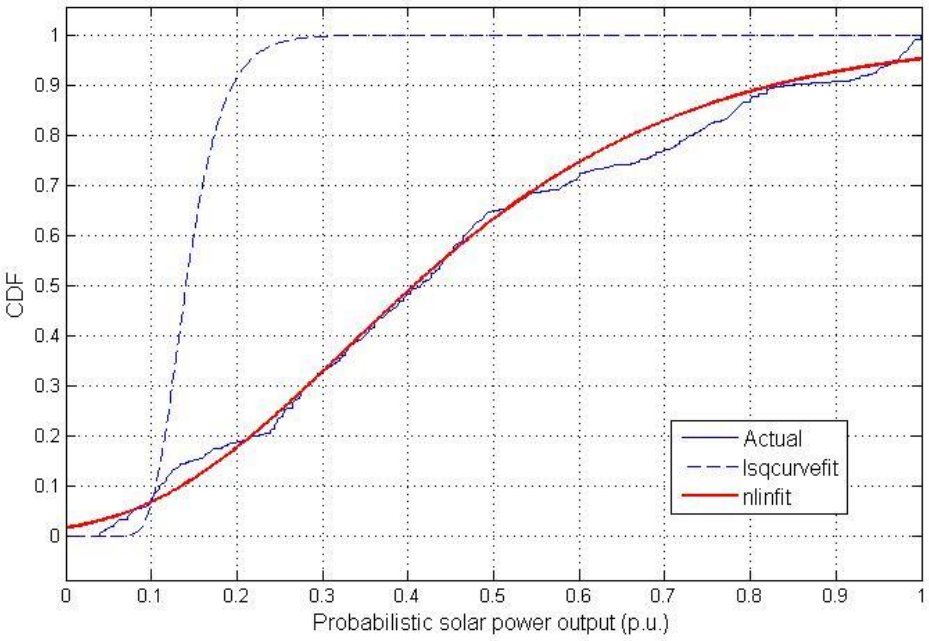

Figure 18 Different curving fitting functions' performance

It is clear that the CDF generated by nlinfit is more accurate than the CDF curve by lsqcurvefit. To verify the accuracy of curve fitting, the actual PDF and versatile PDF is illustrated in following Figure 18.

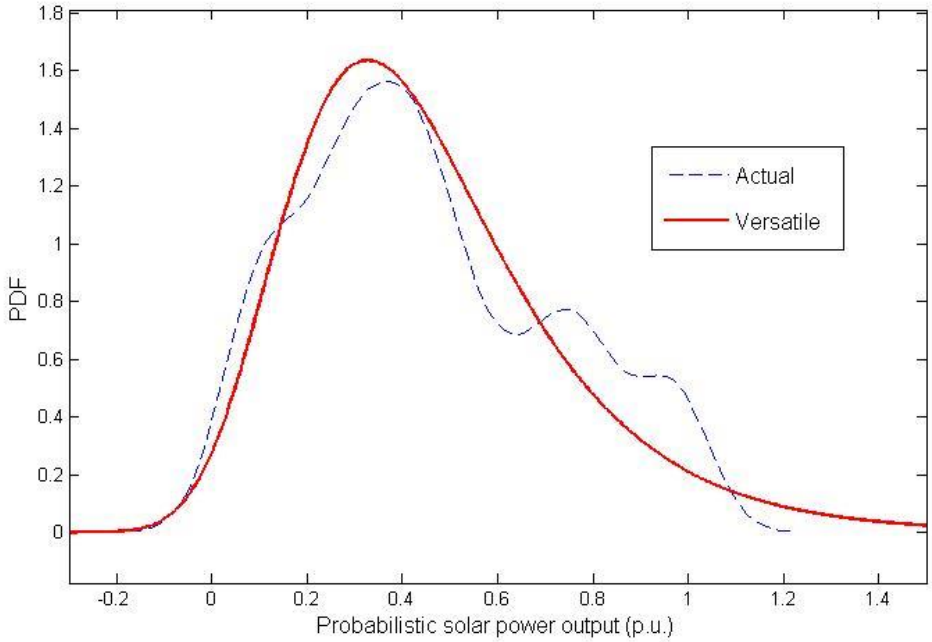

Figure 19 Actual PDF versus Versatile PDF

The versatile PDF fits actual PDF curve reasonably well. The performance and accuracy are both verified in this solar farm case. Similarly, the versatile distribution can be applied to wind farm as well to represent the forecast error in a 15-day forecast span. The simulation results based on actual data [22] are shown in below Figure 20 and Figure 21.

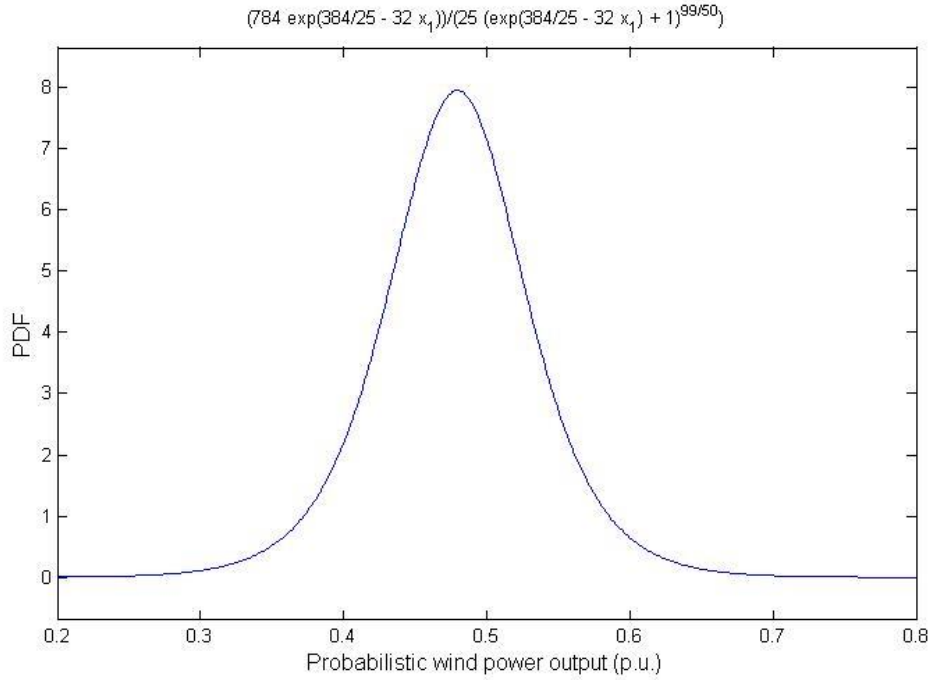

Figure 20 wind farm versatile PDF

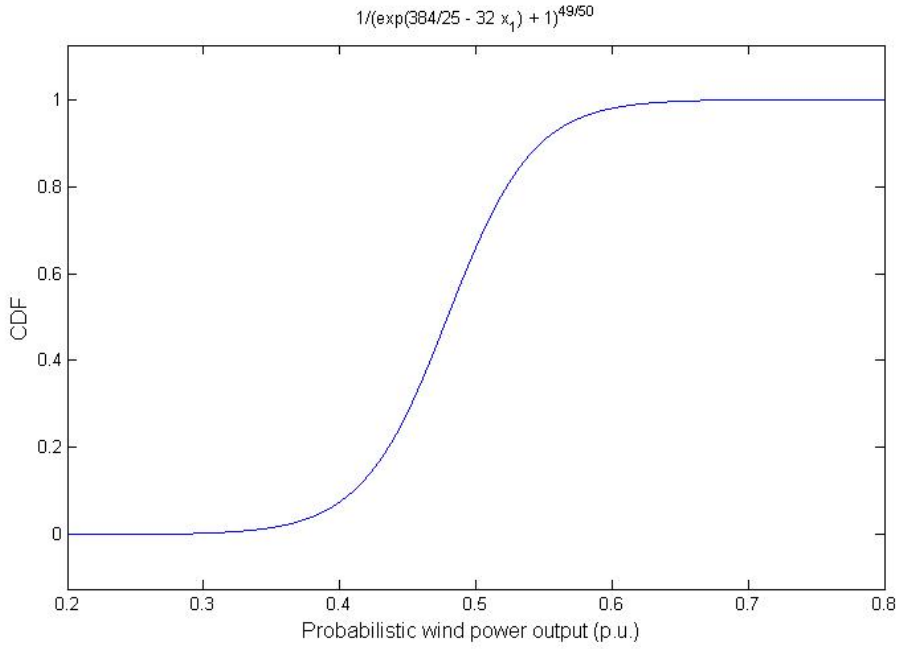

Figure 21 wind farm versatile CDF

1) Wind farm generation cost

Due to the accuracy limitation of wind power prediction, the actual output power can be higher or lower than the predicted output. This inaccuracy will result in operational penalty. The three components (direct cost, overestimation cost, underestimation cost) of wind generation costs are calculated in following set of equations [20].

$$C_{w,j}(w_j) = d_{wj} w_j \quad (27)$$

where

$C_{w,j}$: cost function of wind farm j

w_j: scheduled power of wind farm j

d_{wj}: direct cost coefficient of wind farm j

$$C_{pw,j}(w_{av,j} - w_j) = k_p(w_{av,j} - w_j)$$
$$= k_p \int_{w_j}^{w_{r,j}} (x - w_j) g w_j(x) dx \quad (28)$$

where

$C_{pw,j}$: underestimation cost function of wind farm j

$w_{av,j}$: actual available power of wind farm j

k_p: underestimation cost coefficient

$w_{r,j}$: installed capacity of wind farm j

$gw_j(.)$: PDF of the output of wind farm j for the forecast values

$$C_{rw,j}(w_j - w_{av,j}) = k_r(wj - w_{av,j})$$
$$= k_r \int_0^{w_j} (w_j - x) g w_j(x) dx \quad (29)$$

where

$C_{rw,j}$: overestimation cost function of wind farm j

k_r: overestimation cost coefficient

2) Solar farm generation cost

Similarly, the solar farm shares the same pattern of generation cost of wind farm. However, there is some difference between solar power and wind power. The feasible output period of solar farm is dependent on the actual solar radiation period. In this dissertation, according to actual data [21], the feasible output period is set as from 7 a.m. to 7 p.m. for a 15-day forecast span. Set of cost functions are shown below.

$$C_{s,k}(s_k) = d_{sk} s_k \quad (30)$$

$$C_{ps,k}(s_{av,k} - s_k) = k_p \int_{s_k}^{s_{r,k}} (x - s_k) g s_k(x) dx \quad (31)$$

$$C_{rs,k}(s_k - s_{av,k}) = k_r \int_0^{s_k} (s_k - x) g s_k(x) dx \quad (32)$$

where

$C_{s,k}$: cost function of solar farm k

s_k: scheduled power of solar farm k

d_{sk}: direct cost coefficient of solar farm k

$C_{ps,k}$: underestimation cost function of solar farm k

$s_{av,k}$: actual available power of solar farm k

$s_{r,k}$: installed capacity of solar farm k

$gs_k(.)$: PDF of the output of solar farm k for the forecast values

$C_{rs,k}$: overestimation cost function of solar farm k

5.2 Vehicle to Grid (V2G) Modelling

High amount of charging loads of PHEVs can be a great burden to the whole power grid. However, via vehicle to grid method, the huge energy in PHEVs' battery can supply power back to grid if necessary. Especially in microgrid circumstance, V2G can serve as an energy storage device to smooth out the fluctuation of solar and wind generation. To begin with, some characteristics of PHEVs need to be discussed:

1. Originally, PHEV is a commuting device for all the owners. The charging/discharging procedure need to be conducted with no conflict with owner's daily driving behavior. So, the available time period and capacity is limited corresponding to individual user.

2. The randomness of charging/discharging behavior of each PHEV must be considered.

These characteristics make V2G technology not totally reliable. A great number of PHEVs charging/discharging without planning and order not only increase the pressure on the grid but also waste electricity in the end. As a result, the research about V2G charging/discharging capacity is essential for the following control strategy research.

In the beginning of PHEV development, the total scale and amount of PHEVs is very limited. Compared to the whole system, the impact can be even neglected. However, for microgrid system, comparatively low capacity renewable energy power plants are installed in it. The impact of PHEV cannot be overlooked. The PHEV control center can reasonably utilize the response from all the PHEVs in certain area for peak shaving and valley filling to increase efficiency of energy usage.

In microgrid, power generators can be divided into conventional power plant, fuel cell, PV, wind turbine, and bio energy, etc. To some extent, microgrid can be represented as a combination of several micro energy resources. In the circumstance of microgrid, the system setting needs to take PHEVs into consideration. In the following part, conventional power plant, wind farm, solar farm and PHEV are all included. Hence, a comprehensive optimized strategy can be developed.

Based on the simulation results from [23] and [24], the versatile distribution model of V2G in microgrid is developed. Due to the uncertainty of V2G output, the cost functions consist of three parts: direct cost, underestimation cost, and overestimation cost. The PDF of V2G output from 15 Chevy Volt is shown below.

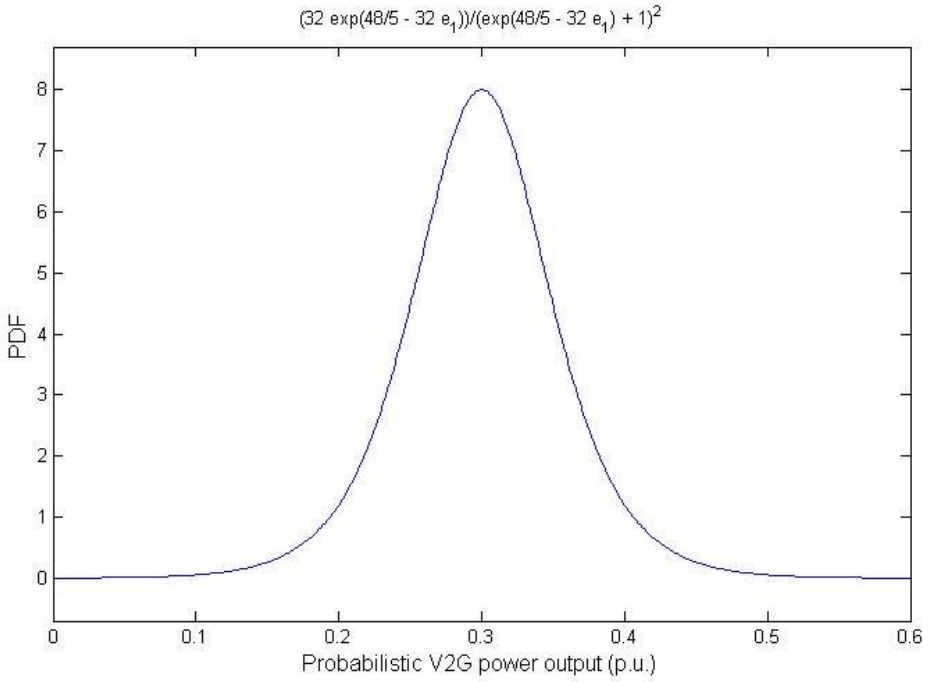

Figure 22 Versatile PDF of V2G power output

5.3 Economic Dispatch in Microgrid

In microgrid, the goal is to minimize the total generation cost. C_{Total} is set as the subtotal generation cost of the whole microgrid system. In this example, C_{Total} includes the generation cost of conventional power plant, wind farm, solar farm, and V2G of PHEVs.

The simulation is based on standard IEEE 33 bus test system. Bus 1 is reference bus.

Objective function (cost minimization)

$$\min C_{Total} = \sum_{i=1}^{I} C_i(p_i) + \sum_{j=1}^{J} C_{w,j}(w_j) + \sum_{k=1}^{K} C_{s,k}(s_k) + \sum_{l=1}^{L} C_{e,l}(e_l)$$
$$+ \sum_{j=1}^{J} C_{pw,j}(w_{av,j} - w_j) + \sum_{k=1}^{K} C_{ps,k}(s_{av,k} - s_k) + \sum_{l=1}^{L} C_{pe,l}(e_{av,l} - e_l)$$
$$+ \sum_{j=1}^{J} C_{rw,j}(w_{av,j} - w_j) + \sum_{k=1}^{K} C_{rs,k}(s_{av,k} - s_k) + \sum_{l=1}^{L} C_{re,l}(e_{av,l} - e_l)$$

(33)

Constraints:

$$\sum_{i=1}^{I} p_i + \sum_{j=1}^{J} w_j + \sum_{k=1}^{K} s_k + \sum_{l=1}^{L} e_l = L \quad (34)$$

$$p_{\min,i} \le p_i \le p_{\max,i} \quad (35)$$

$$0 \le w_j \le w_{r,j} \quad (36)$$

$$0 \le s_k \le s_{r,k} \quad (37)$$

$$0 \le e_l \le e_{r,l} \quad (38)$$

$$\sum_{i=1}^{I} r_{u,i} \ge \sum_{j=1}^{J} (w_j - w_{av,j}) + \sum_{k=1}^{K} (s_k - s_{av,k}) \quad (39)$$

$$\sum_{i=1}^{I} r_{d,i} \ge \sum_{j=1}^{J} (w_{av,j} - w_j) + \sum_{k=1}^{K} (s_{av,k} - s_k) \quad (40)$$

L is the system demand. e_r is installed capacity of PHEV fleet l. $r_{u,i}$ and $r_{d,i}$ are the up and down regulation reserves provided by conventional power plant i. These two constraints represent that the over/underestimation of wind farm output must be covered by up/down regulation reserves of conventional power plant. The cost function of conventional power plant is

$$C_i(p_i) = a_i p_i^2 + b_i p_i + c_i \quad (41)$$

where a_i, b_i, and c_i are fuel cost coefficients of conventional power plant i.

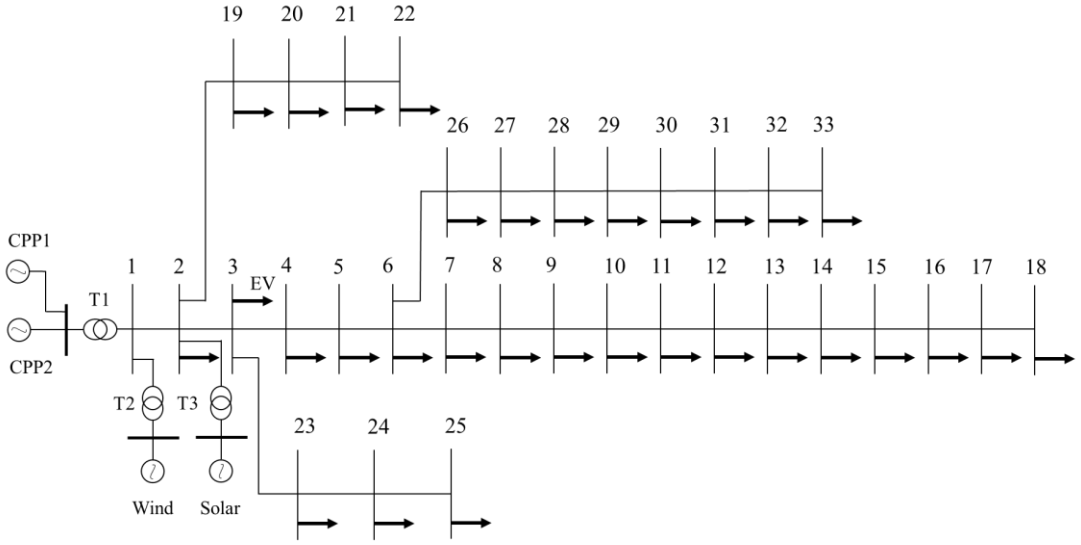

Figure 23 Modified IEEE 33 bus system with PHEVs and DGs

As shown in Figure 23, a 100 kW wind farm and two conventional power plants are all connected to Bus 1. On Bus 2, a 100 kW solar farm is connected to it. The output capacity of both conventional power plants is 100 kW. In this case study, 15 PHEVs are

connected to Bus 3 as the V2G energy source. The rated output is 3.5 kW per vehicle. All generation variables are expressed in per unit. The system power base is 100 kW. The direct cost coefficient of wind power and solar power is 2 $/MWh. For V2G, the direct cost coefficient is 10 $/MWh. The underestimation and overestimation cost coefficients k_p and k_r are set as 1.5 $/MWh and 3 $/MWh [25]. The up regulation reserve is 0.2 per unit. The down reserve is 0.1 per unit. The confidence level c_u and c_d are both set as 0.95. The fuel cost coefficients and output limits for both conventional power plants are listed in Table 12. The parameters of versatile distribution for wind, V2G, and solar are given in Table 13.

Table 12 Parameters of conventional power plants (CPP)

	a ($/h)	b ($/h)	c ($/h)	Pmin (p.u.)	Pmax (p.u.)
CPP 1	100	200	10	0.4	1
CPP 2	120	150	10	0.4	1

Table 13 Parameters of wind, V2G, and solar

	Alpha	beta	gamma
Wind	32	0.98	0.48
V2G	32	1	0.3
Solar	4.48	55.98	-0.57

Since the inverse CDF of versatile distribution has analytical form, the optimization problem can be linearized and solved by Sequential Linear Programing

(SLP). Detailed procedure can be found in [19] and [20]. The simulation results are shown in Figure 18. P1 and P2 are two conventional power plants' outputs respectively. S1 is solar farm output. E1 is V2G output. X1 is wind farm output. There are two obvious load peaks around noon and around evening. The load peak at 8:00 a.m. is 2.9 per unit. And the peak load of all day is 3.37 per unit at 6:00 p.m. From Figure 19, it can be figured out that V2G participates in power generation at 6, 7, and 8 p.m. These time points are also in load peak period in which V2G can be a quick responsive power source to dispatch in microgrid.

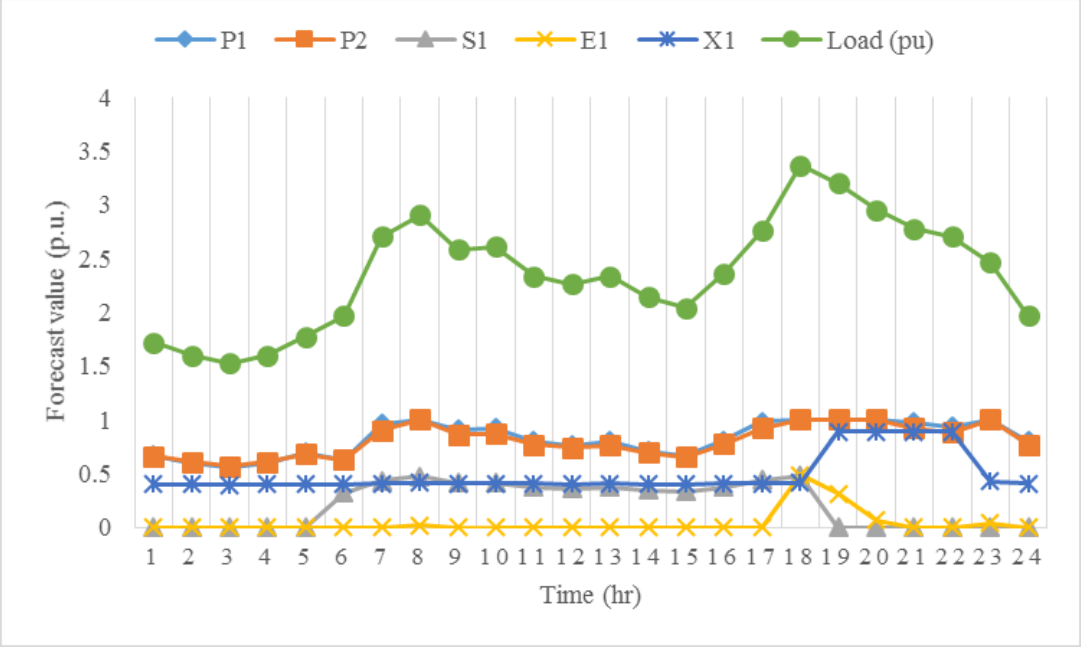

Figure 24 Forecast value of all micro power sources (CPP: P1, P2 Solar: S1 EV: E1 Wind: X1)

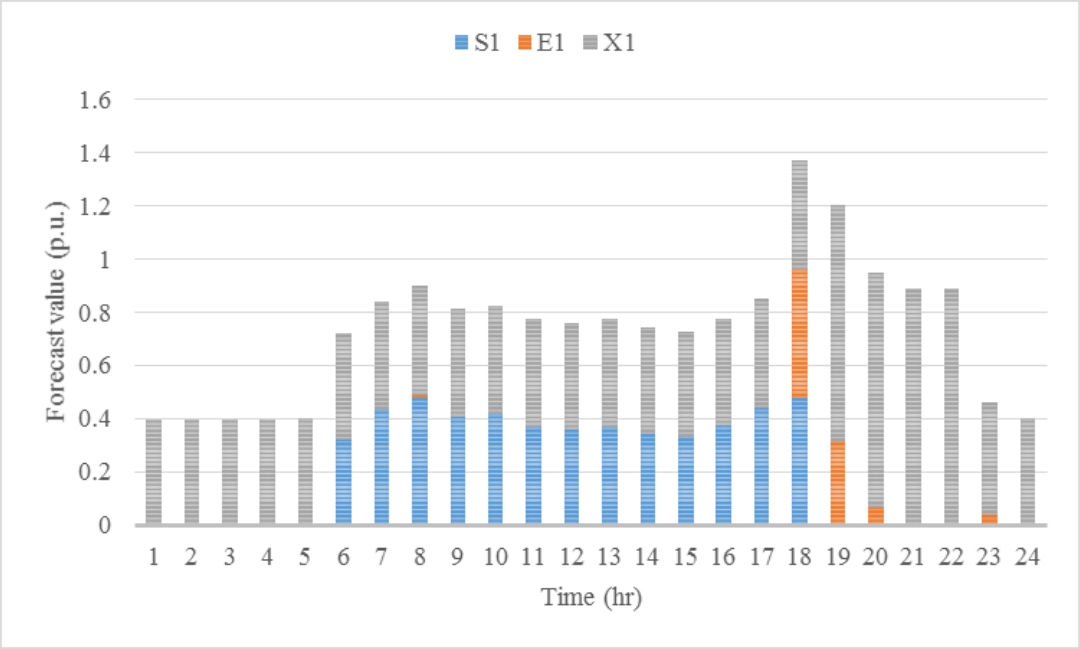

Figure 25 Output value of wind, V2G, and solar (Solar: S1 EV: E1 Wind: X1)

In Chapter 1, a versatile distribution model is utilized to forecast the output error for wind farm, V2G, and solar farm. Then, the probabilistic distribution models are applied to economic dispatch problem in microgrid. From the IEEE 33 Bus case study results, it reveals that V2G can serve as a quick responsive energy source to accommodate peak loads. As a result, the power quality in microgrid can be improved.

In conclusion, transportation electrification in microgrid will surely become more and more critical in distributed generation. Since the main energy sources in microgrid are wind and solar farms in future, the microgrid system always needs a reliable and responsive power source. V2G can be a favorable option with the increasing penetration

level of PHEVs. On the other hand, V2G is able to help microgrid become more independent of external power grid.

Chapter 6. Optimization in Generation Side

6.1 Charging Load Schedule Optimization Referring to Real-time Pricing

Smart grid and smart meter make it possible that costumers could know real time electricity price before they use. Consequently, this will give them a strong incentive to charge their PEV when price is low or even sale electricity from vehicle to grid (V2G) to make money when the price is high.

As to taxis and buses, they might get notice from operation center to suggest them charge battery when price is low. For instance, they might bring forward a break to charge battery at low price to save money. Since their daily mileage is far more than that of private vehicle. The cumulative saving is considerable. Furthermore, shift load peak would relief the stress on the grid at noon and midnight.

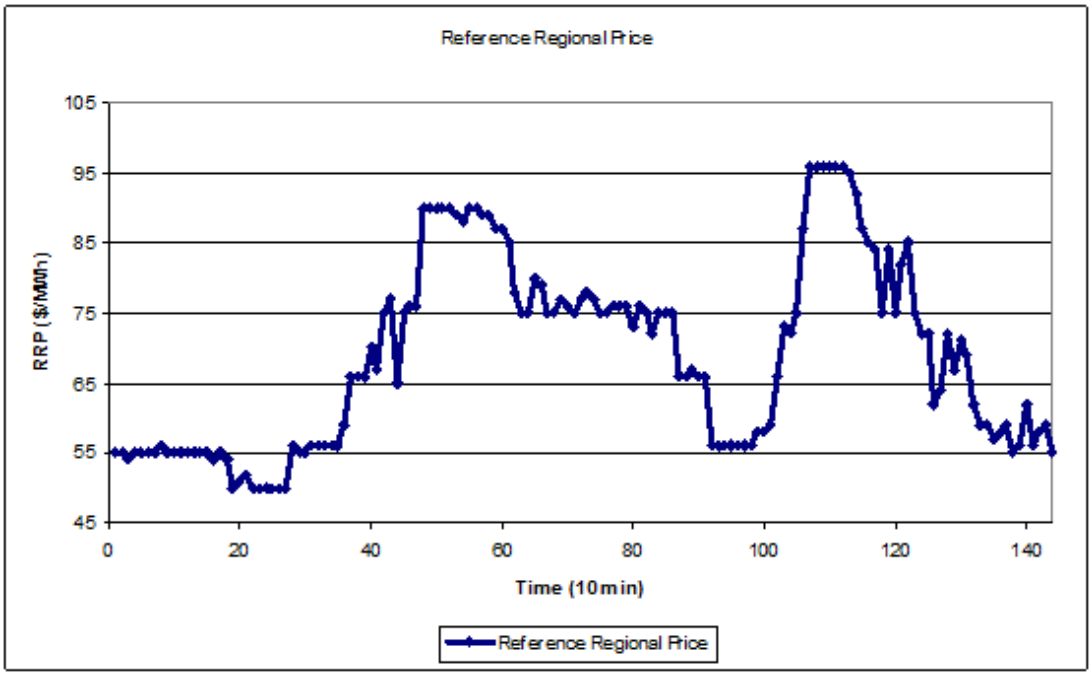

Figure 26 Reference regional price curve [22]

Here is a reference regional price curve in 7/8/2012. There are two obvious price peaks in the morning and evening. The morning peak is from 50 to 65. The reference regional price is about $90 per MWh. The evening peak is quite short. It is from 107 to 116. The peak value is about $95 per MWh.

The optimization's goal is shift loads from these two areas to valley areas. Real time price usually implies the total demand of this region. So, when the price is high, it means total demand is at high level and system needs the help from high-cost facilities. If loads could be shifted from these peak areas, this act could relief the pressure on the grid and prevent new price peak in this area. Another advantage is obvious. Owners of PHEVs

could save money on electricity bill. On the other hand, their batteries are still charged as much as possible.

Compared to the real-time pricing schedule, it is obvious that charging loads all locate at the time period that the price is low. If we compare the optimized results with original simulation results, it is clear that loads in morning peak area are shifted to right. Similar optimization method could also be applied to taxi charging pattern and private vehicle charging pattern.

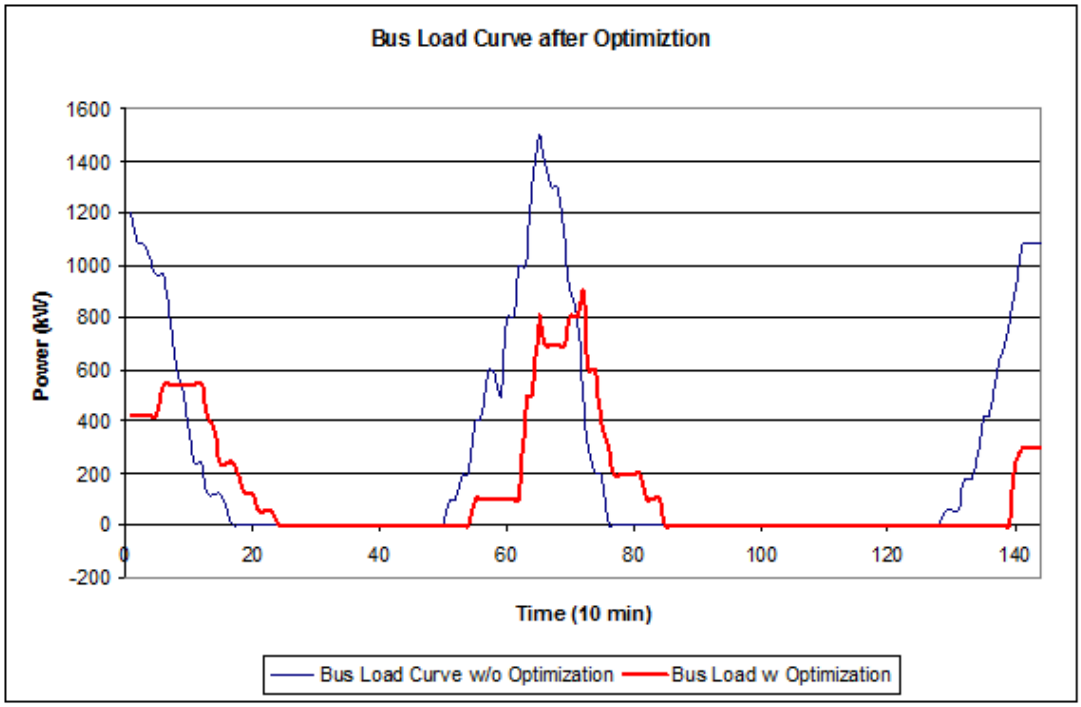

Figure 27 Bus load curve after optimization

Similar optimization method could also be applied to taxi charging pattern and private vehicle charging pattern.

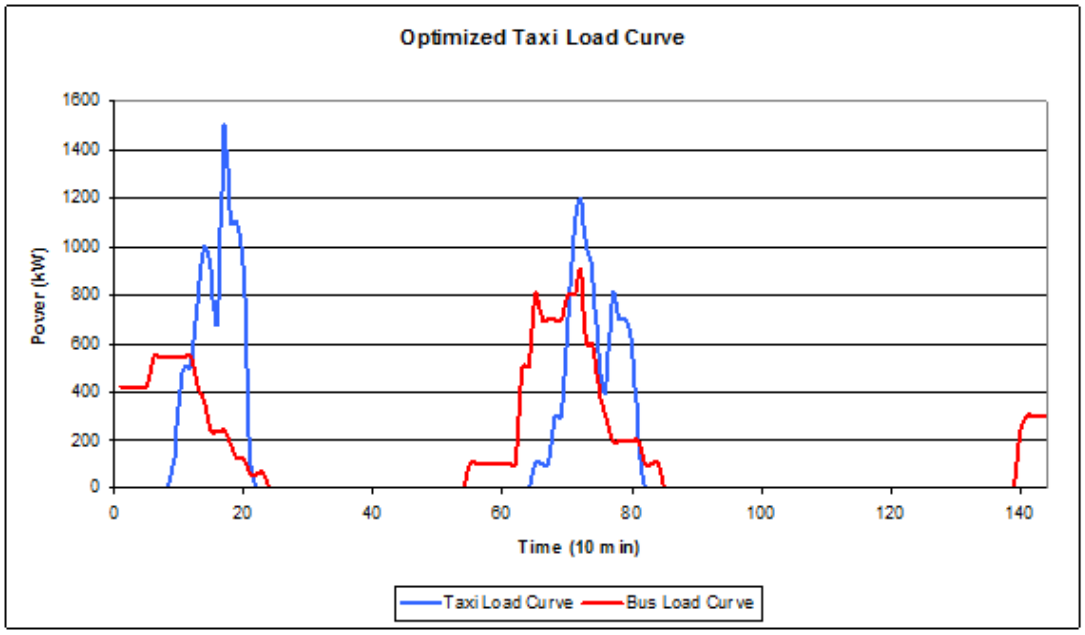

Figure 28 Optimized taxi load curve

Similar to the results of electric bus, load of taxi also lies in the area where real time price is low. That also reveals that there is great potential for taxi load operation.

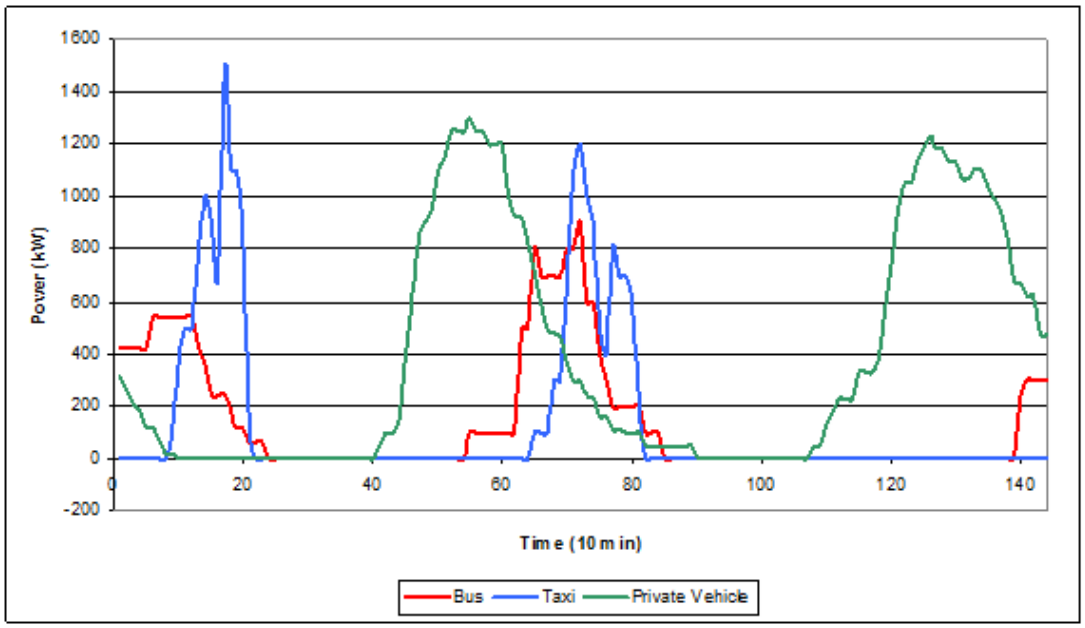

Figure 29 Optimized load curve for 3 types of vehicles

From Figure 29, it is clear that private vehicle was shifted rightwards. After the load peak, load curve decreases gradually until 15:00 o'clock in the afternoon.

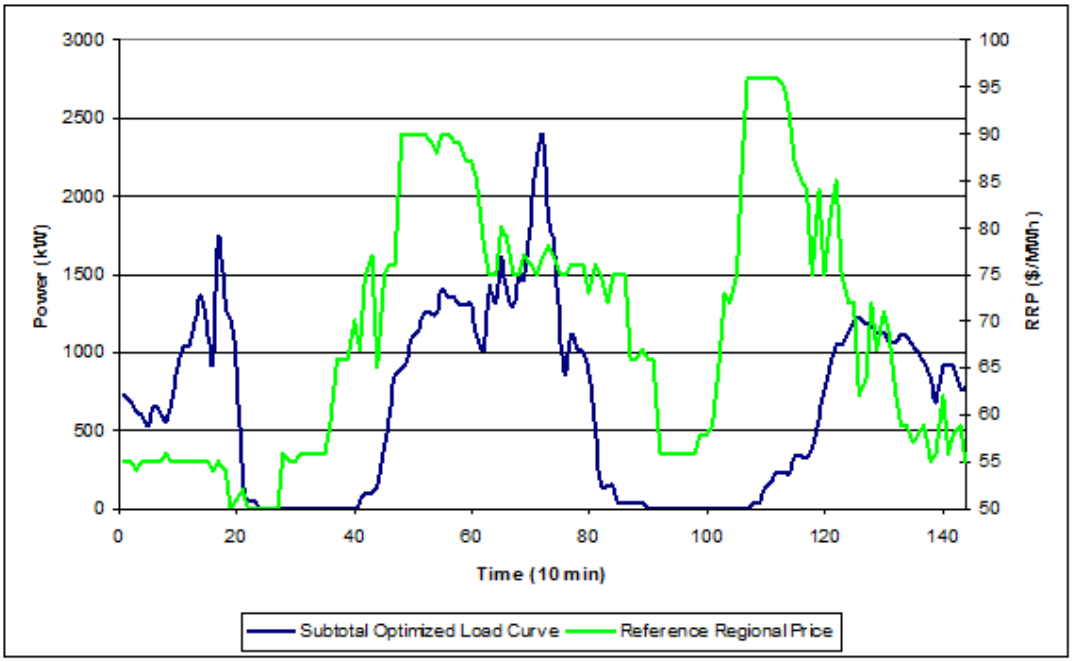

Figure 30 Optimized total load curve compare to RRP curve

The overall load patter for three types of vehicles after optimization according to real-time pricing is shown in Figure 30. We may recall the results from small scale simulation, loads suddenly drops to zero after 11:30. However, in optimized load curve, loads allocate more evenly, and loads decrease to zero until 15:00. That means loads were shifted to afternoon successfully.

6.2 Charging Load Schedule Optimization Referring to Renewable Power Output

Besides real-time pricing, if wind output curve is also considered in objective function, excess wind power could be better utilized. The reasons why wind power should

be coordinated with PHEV charging are as follows: (1) as is known to all that it is hard to control wind power output. Wind farm may suddenly generate many megawatts of power or drop to zero output in ten minutes. That is always a risk for voltage and frequency stability. Normally, if wind farm output increases abruptly, operation center will have to decrease generation from other power plants to maintain the balance. Now, charging loads join the grid and when to charge these loads could be controlled since their charging time is pretty ample. These loads could be utilized to pick up this increase from wind farm without shutting down other power plant. (2) A lot of wind power in midnight is just wasted, and charging loads in midnight is able to utilize this excess power. (3) PHEV is friendly to environment. If electricity is also from clean energy, that means there is no carbon dioxide emission from energy source to every vehicle terminal.

Wind power output curve on 1/1/2011 is illustrated in Figure 31 [22]. The variability for wind power output is considerably large. The output is at high level from 0:00 to 15:00 and suddenly drops to zero. Nowadays, there are many methods to predict wind power output. If the predicted load curve could be utilized in optimization, which would surely help to better take advantage of wind power.

Main objective function

$$J = P_1 \cdot \sum_{m=1}^{m=N} \sum_{t=X_m}^{t=X_m+Tc_m} p[t] + P_2 \cdot \sum_{m=1}^{m=N} \sum_{t=X_m}^{t=X_m+Tc_m} w[t] \qquad (42)$$

$$Tc_m = (1 - SOC_m) / CS_m$$

Constraints

$$X_m \geq At_m$$
$$0.2 \leq SOC_m \leq 1$$

$$p[t] = \frac{P[t] - Min\{P[t]\}}{Max\{P[t]\} - Min\{P[t]\}}$$
$$w[t] = \frac{W[t] - Min\{W[t]\}}{Max\{W[t]\} - Min\{W[t]\}}$$

W[t] is the wind power output curve. This output curve is from a 72 Mits Wind farm on 1/1/2011. P[t] is the reference regional price curve. Since regional reference price curve and wind power output curve are not on the same scale, all of them should be normalized in order to assign similar importance to each one. P_1 and P_2 are two constants. $P_1 + P_2 = 1$. Operator may assign different values for P_1 and P_2 to lay more emphasis on real-time pricing or wind power output.

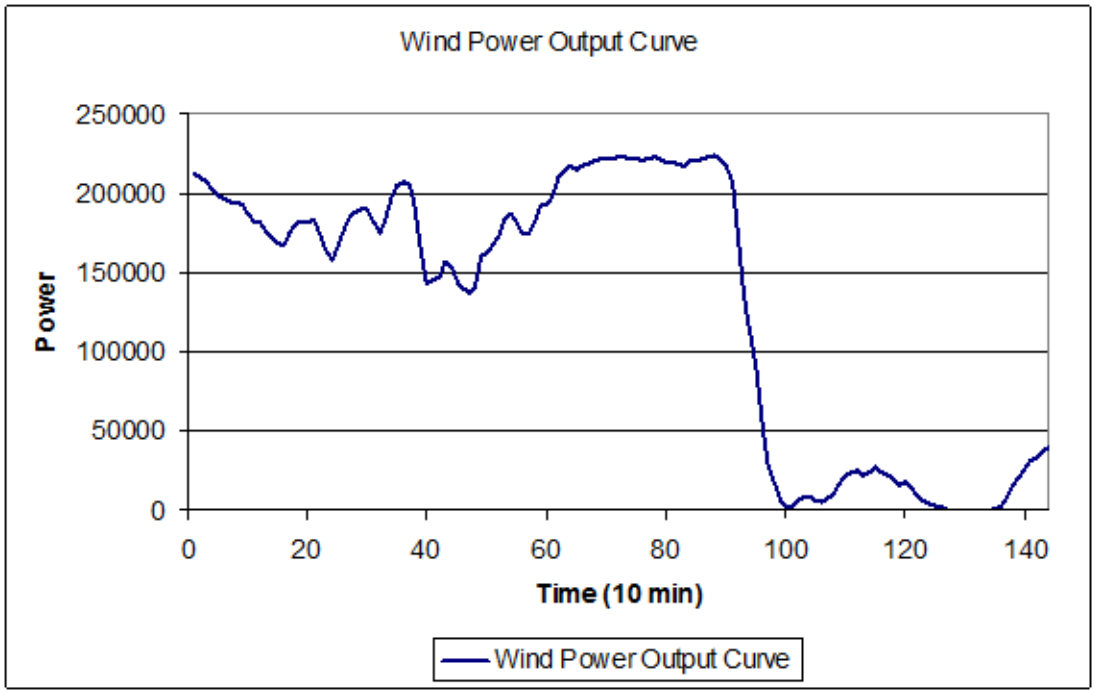

Figure 31 Wind power output curve on 1/1/2011

Considering wind power output curve, more vehicle charging loads were fulfilled when wind output is high. In Figure 31, the most productive area for wind power is from 60 min to 80 min. Compared to load curve without considering wind power, loads in this area increase to some extent clearly. In future work, besides wind power, solar power and other factor could also be taken into consideration. That would grant the operator more potential to optimize the charging pattern for PHEVs.

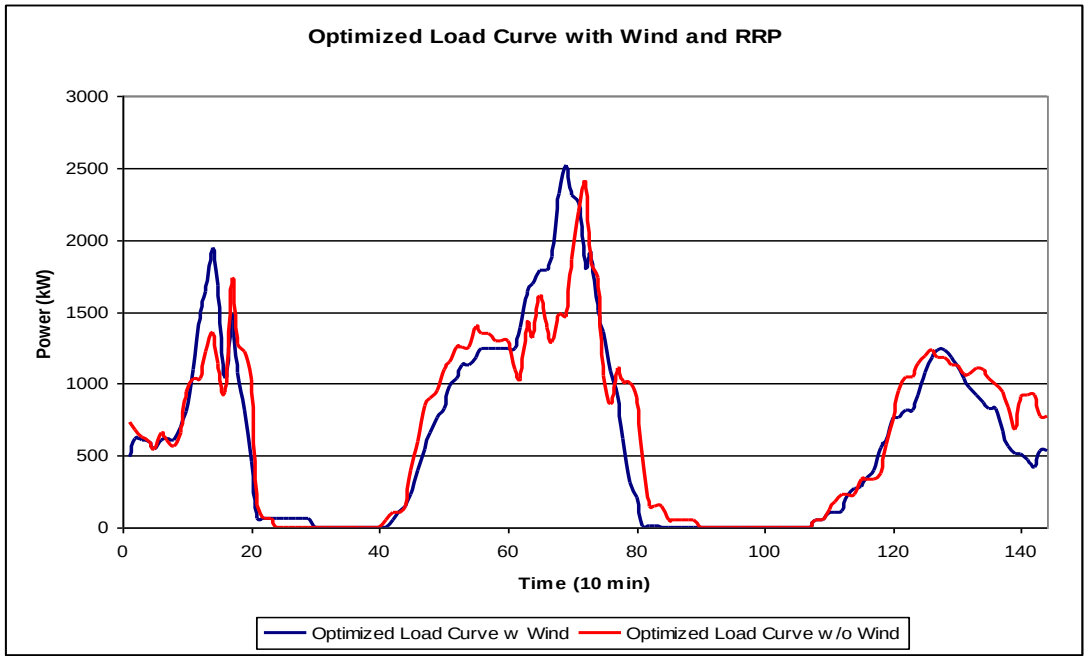

Figure 32 Optimized load curve with wind and reference regional price

6.3 Charging Load Schedule Optimization Referring to Output from Hybrid Wind System

◆ SOC feedback control of wind power/battery energy storage system

In this section, hybrid wind power/battery energy storage system would be introduced. Compare to the normal WF, a battery energy storage system (BESS) is installed to smooth out the fluctuation of the total WF output [26]. BESS could supply power to the WF or get charged from it according to the Target Output signal. Figure 33 shows the outline for BESS control. WF output data goes through a First Order Lag Filter to produce a Target Output with a time constant T (T is called smoothing time constant).

Then, the difference between WF output and Target output would be value that BESS should supply or absorb via an AC-DC converter. Ideally, if the capacity and charge/discharge power of BESS is large enough, the Smoothed output that consists of BESS output and WF output could be constant. That means the fluctuation of the WF output is perfectly smoothed out. However, in real life, the perfectly smoothed output is not practical due to the cost of battery packs and other limitations.

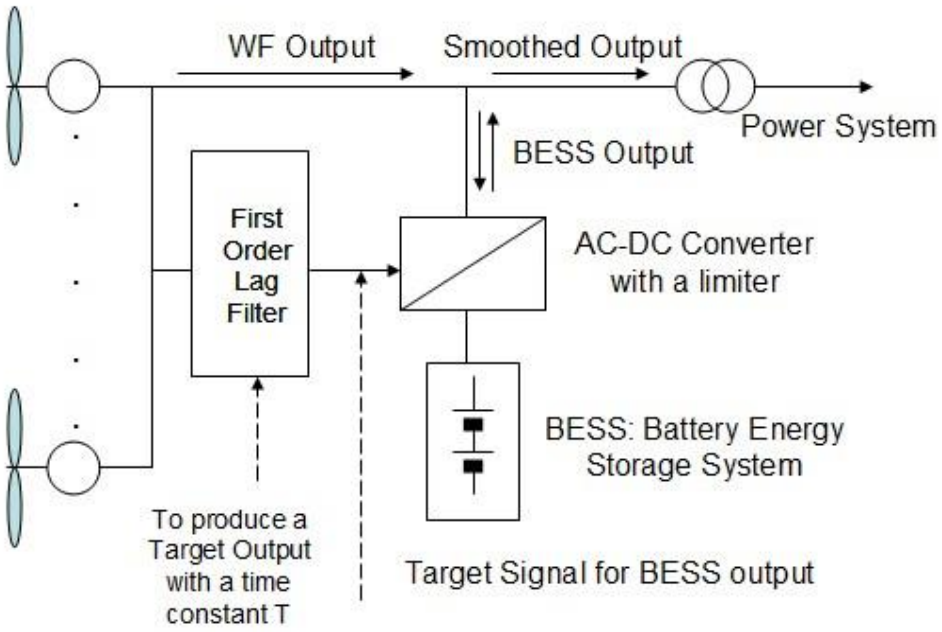

Figure 33 Hybrid wind power/battery energy storage system

The Target output, BESS output and Remaining Energy level (REL) of the battery are determined by the following functions. REL is the percentage of energy that remains in the battery.

$$\text{Targe Output}: O_0(s) = \frac{1}{1+sT} G(s)$$

$$\text{BESS Output}: H_0(s) = \frac{1}{s+sT} G(s) - G(s) = \frac{-sT}{1+sT} G(s) \quad (43)$$

$$\text{REL of the battery}: I_0(s) = \frac{-H_0(s)}{s} = \frac{T}{1+sT} G(s)$$

G(s) is the total WF output. $O_0(s)$, $H_0(s)$ and $I_0(s)$ are output values without SOC feedback control. To avoid overcharge or deep discharge cases, a SOC feedback (SOC-FB) loop is added to monitor the battery status. The block diagram of hybrid wind power/battery energy storage system with SOC-FB control is shown in Figure 34.

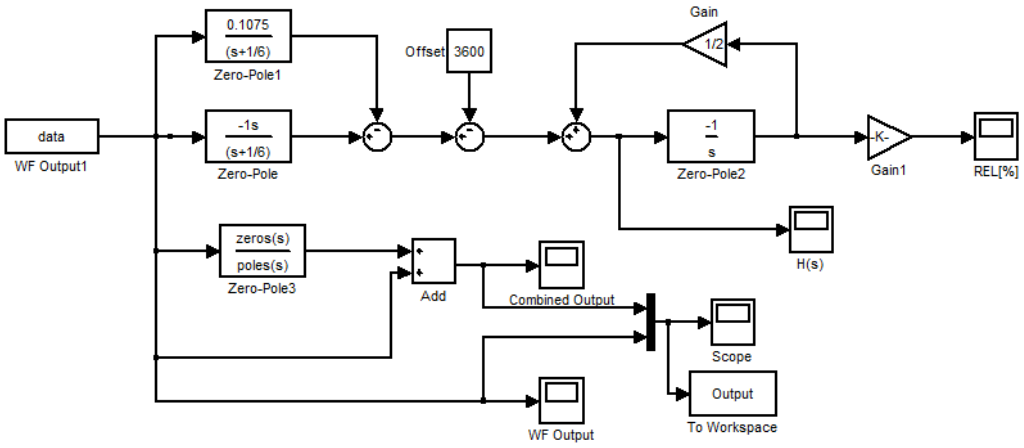

Figure 34 Block diagram of SOC-FB control system

The REL, I(s) can be determined by following equation

$$I(s) = \frac{s + AB/T}{s + A} \cdot \frac{1}{s + 1/T} G(s) + \frac{A(E - BC_{WF})}{2} \cdot \frac{1}{s + A} \quad (44)$$

where

A (sec^{-1}): Feed back gain

B= αT (sec): Target output gain

E (kWh): Battery rated capacity

C_{WF} (kW): WF rated output

Simulation parameters

1. WF

Max WF output = 16.972 MW, 12 Mitsubishi wind turbines

2. BESS control system

24 hours, Max BESS power output = 6000 kW, Capacity of battery = 60000 kWh

T= 60 min, A = 1/T, Margin rate = 10%

3. Initial condition

When t = 0, Target output = WF output

REL (%) = 0%

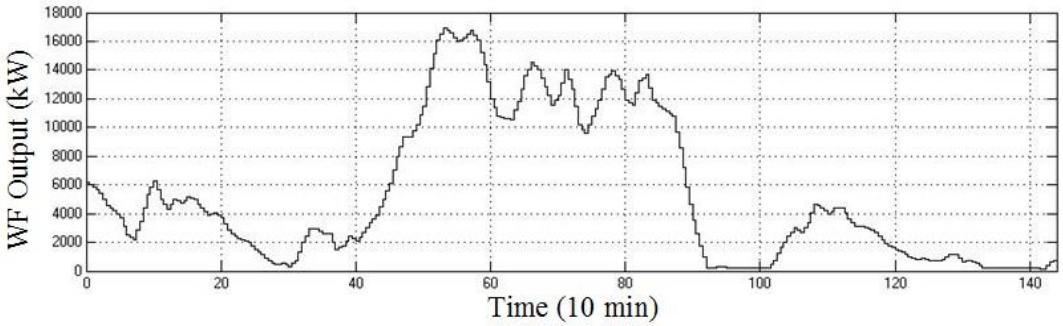

Figure 35 WF output

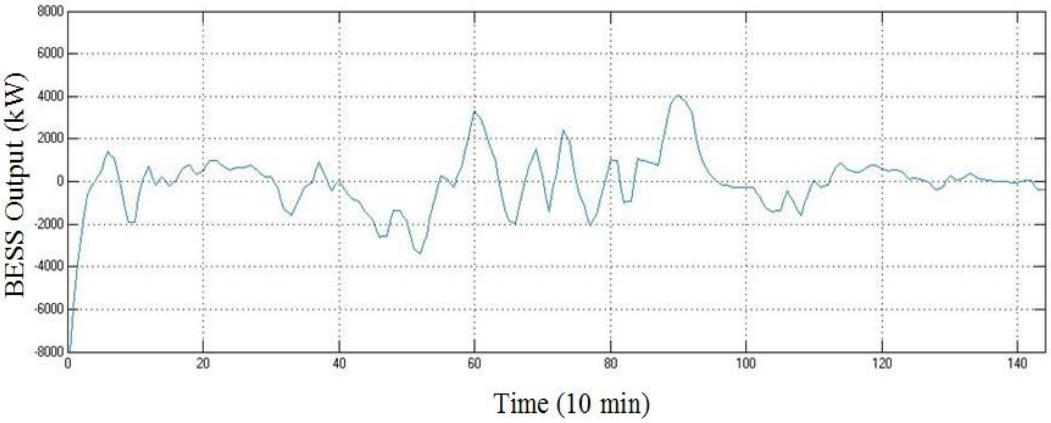

Figure 36 BESS output

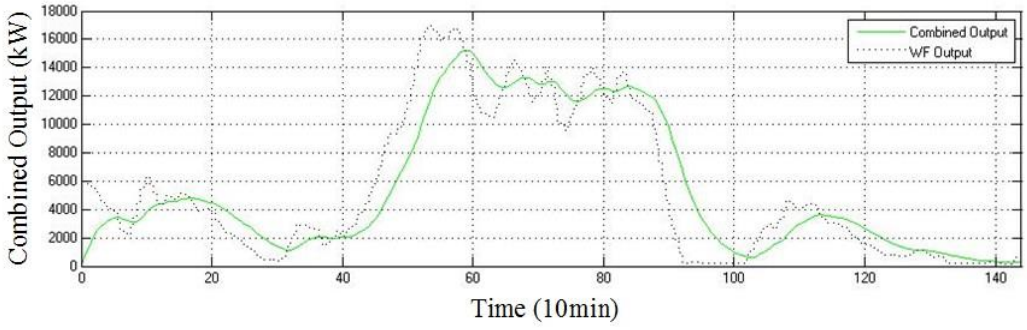

Figure 37 Combined output of hybrid system

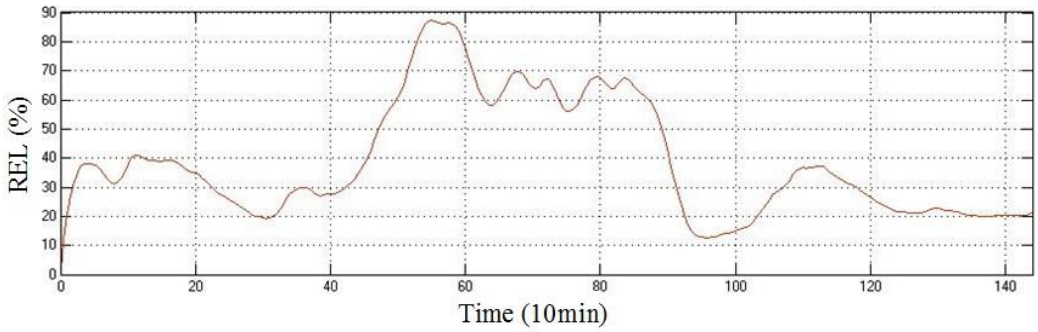

Figure 38 Remaining energy level of the battery pack

In Figures Figure 35~Figure 38, 10 minutes is the unit for time axis. It could be easily figured out that the output of the hybrid system is much smoother than the original WF output curve. For instance, the minimum value of WF output is only 152.66 kW at 11:40 p.m. BESS helps to mitigate the variations and increase the minimum value to 546.47 kW. On the other hand, from Figure 38, the REL of BESS is controlled in a proper range (10%~90%). Deep discharging and over charging are prevented to maximize the battery lifetime.

Taking into account the wind power output curve, more vehicles charging loads are fulfilled when the wind output is high. In Figure 39, the most productive area of wind power is from 8:00 a.m. to 3:00 p.m. Compared to the load curve without considering wind power, loads in this area increase to some extent clearly, which means wind power is better utilized. On the other hand, if smoothed wind output data is applied, the optimized load curve would become smoother and load peaks decrease evidently as shown in Figure 39.

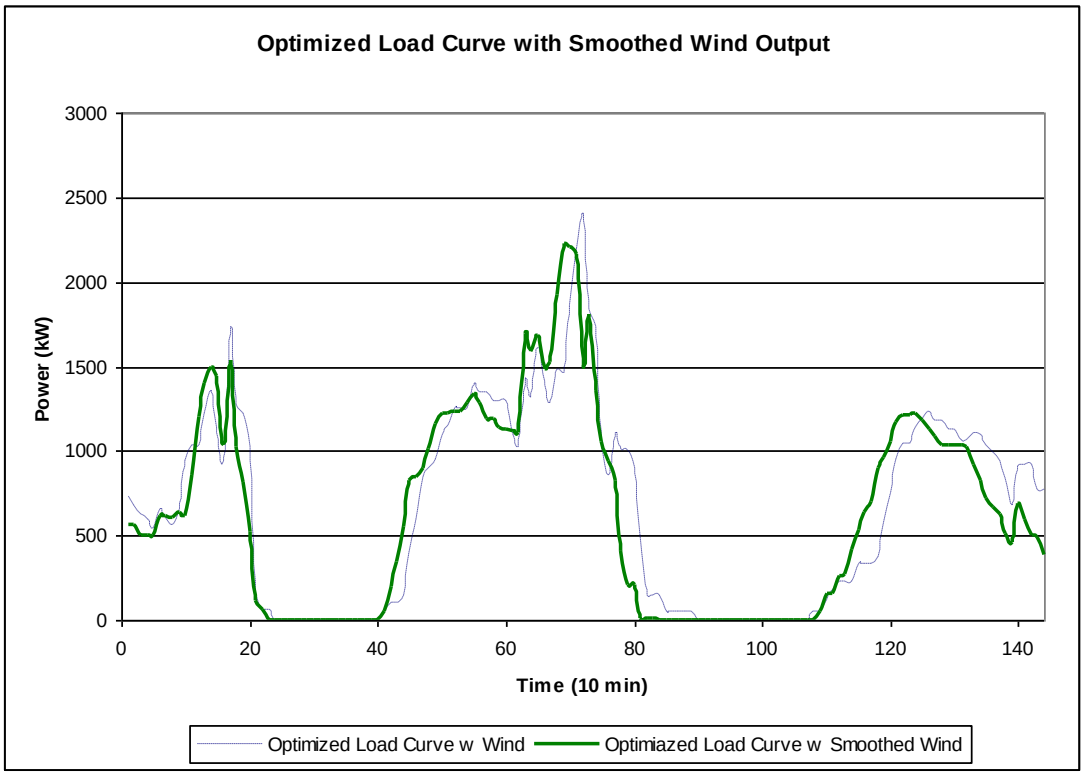

Figure 39 Optimized load curve w and w/o smoothed wind

Chapter 7. Economic Potential of Schedule Optimization

7.1 V2G Capacity Prediction

With the growing trend of PHEV market, high amount of PHEVs plugged into the grid simultaneously surely will lay a great impact on both stability and economics of the whole power system. In some research papers, they describe this certain level of PHEV charging as an enormous burden to the grid. That is the reason why V2G tech is meaningful under this circumstance. Since PHEVs are treated as generators when the bulk energy in PHEVs is more than sufficient.

However, with the participation of PHEVs in power dispatch of the microgrid, some characteristics of PHEVs need to be mentioned

1. PHEV is a commuting device for all the users originally. The charging/discharging procedure need to be conducted with no confliction with user's daily driving behavior. So, the available time period and capacity is limited corresponding to individual user.

2. The randomness of charging/discharging behavior of each PHEV must be considered.

These characteristics make V2G tech not that reliable. A great number of PHEVs charging/discharging without sequence and order not only increase the pressure on the grid but also waste electricity in the end. As a result, the research about V2G charging/discharging capacity is essential for the following control strategy research.

In the beginning of PHEV development, the total scale and amount of PHEVs is very limited. Compared to the whole system, the impact can be even neglected. However, for microgrid system, comparatively low capacity renewable energy power plants are installed in it. The impact of PHEV cannot be overlooked. The PHEV control center can reasonably utilize the response from all the PHEVs in certain area for peak shaving and valley filling to increase efficiency of energy usage.

In microgrid, power generators can be divided into conventional power plant (CPP), fuel cell, PV, wind turbine, and bio energy, etc. To some contend, microgrid can be represented as a combination of several micro energy resources. In the circumstance of microgrid, the system setting needs to take PHEV into consideration. In the following part, CPP, wind farm, battery pack and PHEV are all included. Hence, an optimized strategy can be generated.

7.2 Dispatch Strategy of V2G in Microgrid

To decrease the effect of large amount of PHEVs charging/discharging simultaneously and to avoid the loss of life (LoL) increases due to charging/discharging frequently, an optimized dispatch strategy needs to be developed with the participation of PHEVs into microgrid.

1. Direct control: Microgrid stays in the leading role. It send signals to PHEVs and let them charging/discharging at certain requirement of the system.

2. Indirect control: Both microgrid and PHEVs have the same priority. PHEVs made decisions due the real time price of electricity from the system. They can sell at high price and purchase at low price.

However, compared to the first control strategy, it is hard to make it practical. In this research, first method is adapted. To enforce the direct control strategy, both sides must follow below agreements.

1.Plug-in time point of PHEVs

The driving behavior of different type of PHEVs has already been covered in Section 6.2. The results of simulation reveals that there would be to charging peaks in 24 hours. One moon peak and one evening peaks. According to driving behavior simulation, it also reveals that there would be great potential to shift the peak loads to valley area.

2.Payment from microgrid to PHEVs

If PHEVs supply services to microgrid, the operator of microgrid needs to pay owners of PHEVs service fee. The amount of service fee depends on the capacity of PHEV's battery.

3.Energy trading price

There would be energy trading between PHEVs and microgrid when PHEVs supply power. The sell price must be higher than purchase price to motivate PHEV owners to make money by V2G service. For the microgrid side, the purchase price from PHEVs need to be lower than the purchase price from the grid. Under these two conditions, this is a win-win situation for both PHEV owners and microgrid.

7.3 Economic Analysis Model of Microgrid with V2G

The economy of microgrid includes initial fixed investment and operation cost. For the fixed investment, it mainly depends on the type and number of energy resources that going to be used in this microgrid. Referring to load prediction results, the cost of power output in microgrid can be calculated considering installed capacity and operation cost. In this studied microgrid system, CPP is set as the critical core. It is responsible for heating in winter and cooling in summer and partially dispatch certain amount of load. With this strategy, the efficiency of energy utilization is improved.

1. Operational cost from fixed investment

In microgrid, the fixed investment for micro energy source includes purchasing expense, operational life span, maintenance cost, and the amount of micro energy source, etc. Four types of common micro energy sources are listed in below table.

Table 14 Micro energy sources

Type	Rated Output (kW)	Purchasing Expense ($/per)	Maintenance cost ($)	Operational Life Span (Yr)
CPP	65	20000	1000	10
WT	60	25000	1250	15
PHEVs	3.5	-	-	-
PV	60	25000	1300	15

The annual cost function of purchasing, maintenance, and life span for each micro energy source is shown below.

$$C_f = C_{inv} \cdot \frac{r(1+r)^{\alpha i}}{(1+r)^{\alpha i} - 1} + C_{mend} \quad (45)$$

C_f is the annual operation cost of a micro generator. C_{inv} is the purchase cost. C_{mend} is the maintenance cost. r is the interest rate. α_i is the expected life of micro generator. $\frac{r(1+r)^{\alpha_i}}{(1+r)^{\alpha_i} - 1}$ is the coefficient of return on investment.

From above, the annual running cost of microgrid is

$$C1 = \sum_{i=1}^{n} N_i \cdot C_f \quad (46)$$

N_i is the amount of certain type of micro generator. C_1 is the running cost of microgrid in response to loads.

2. Operational cost from dispatching load

The energy source for wind farm is wind. Wind is no cost and renewable for human. The maintenance cost for wind turbine is comparatively low as well. So, in microgrid, wind farm is preferred to stay in maximum output status. In condition that it cannot dispatch load individually, micro gas turbine and PHEVs may substitute to cover

the shortfall between load and output. Purchasing electricity from nearby microgrid is also an optional in deregulated power system.

The operational cost function from dispatching load for each energy source in everyday is shown below

$$C2 = \sum_{i=1}^{24} (C_{mti} \cdot V_{mti} + C_{i,mt}) + (C_{pchs} - C_{sell}) + (C_b - C_s) \quad (47)$$

C_{mti} is the price of natural gas, V_{mti} is the volume of natural gas that be consumed by micor gas turbine i. C_{pchs} is the cost of electricity purchase from external network. C_{sell} is the profit of selling electricity to external power grid. C_p is the cost of electricity purchase from PHEV control center. C_s is the profit of selling electricity to PHEV control center. In island condition, $C_{pchs} = C_{sell} = 0$.

The subtotal cost for the entire microgrid daily is

$$C = \frac{1}{365} \cdot C1 + C2 \quad (48)$$

Objective function is to minimize the subtotal operational cost daily:

Min(C)

Constraints

The constraints in microgrid includes power dispatch balance, micro gas turbine output, wind farm output, and PHEVs charging, discharging constraints, etc.

1) Power dispatch balance

To achieve the balance between generation and load, the output from different type of power source need to subject to following equation.

$$P + \sum_{i=1}^{n_w} P_{wi} + \sum_{i=1}^{n_e} P_{ei} + \sum_{i=1}^{n_{mt}} P_{mti} + \sum_{i=1}^{n_s} P_{si} = L + D \quad (49)$$

P_{wi} is the output from wind farm. P_{ei} is the output from PHEVs. P_{mti} is the output from micro gas turbine. P is the trading power from power market.

2) Constraints for wind farm output

For safety consideration, the maximum wind farm output need to be restricted.

$$P_{wi,\min} < P_{wi} < P_{wi,\max} \quad (50)$$

3) Constraints for micro gas turbine output

$$P_{mti,\min} < P_{mti} < P_{mti,\max} \quad (51)$$

4) Constraints for micro gas turbine output

$$P_{si,\min} < P_{si} < P_{si,\max} \quad (52)$$

5) Constraints for PHEVs output

PHEVs can both consume or supply power from micro grid. If PHEVs are charging their battery, P_e is negative. If PHEVs are discharging battery to supply power back to system, P_e is positive.

Charging condition

$$0 < P_{ei,dis} < \min[P_{dis,N}, (SOC_{ij} - SOC_{\min})] \quad (53)$$

Discharge condition

$$-\min[P_{c,N}, (SOC_{\max} - SOC_{ij})] < P_{ei,c} < 0 \quad (54)$$

SOC_{ij} is the state of charge for i th PHEV in time j. SOC_{min} is the minimum state of charge. It is set to 0.2 to prevent the battery from over discharging. SOC_{max} is the maximum state of charge. To protect the battery from overly charge and damage the

battery life span, it is set to 0.9. $P_{ei,dis}$ is the discharging power for *i* th PHEV. $P_{ei,c}$ is the charging power. $P_{c,N}$ is the rated charging power. $P_{dis,N}$ is the rated discharging power.

7.4 Case Study – Minimize System Operation Cost

Simulation method

In this section, PSO will still be employed to optimize the load allocation. The main procedure is shown below.

1) Initialize the particle velocity, location and sufficiency

2) Generate wind speed, charging/discharging power value from probabilistic distribution via Monte Carlo method. Check whether satisfy all the constraints afterwards. Obtain the position and speed for initial particle swarm that is feasible.

3) Calculate the sufficiency function for each particle

4) Compare the sufficiency value with local optimized value. If it is better, then update the local optimized value.

5) Compare all the sufficiency values with global optimized value. If any of it is better, then update the global optimized value.

6) Update particle location and speed, check the constraints again. If constraints are not all satisfied, speed and location of particle need to be updated again till all constraints are met. Repeat step 3) to 6) till the final solution is obtained.

7) Generate global optimized solution.

Method improvements

1) The inertia weight

The optimized expectation for PSO is high global searching performance in initial stage, and in later stages, the local searching performance is strong. From function aspect, w(k) may increase or keep constant at initial stage and begin to decrease gradually afterwards.

$$w(k) = w_{start} - \frac{w_{start} - w_{end}}{K} k \quad (55)$$

K is the up limit of iterations, *k* is the current number of iterations.

2) Learning factor

The purpose of learning factor is to enhance the performance in global optimized solution searching. In the whole process, learning factor *c1* decreases while learning factor *c2* increases. The effect of this learning factor is that the particle can go through the whole searching area in the beginning. While in later stage, particle is more likely to direct to global solution.

$$c1(k) = c1_{start} + \frac{c1_{start} - c1_{end}}{K} k$$
$$c2(k) = c2_{start} + \frac{c2_{start} - c2_{end}}{K} k \quad (56)$$

where

$c1_{start}$ and $c1_{end}$ are two constants for *c1*'s initial and final value

$c2_{start}$ and $c2_{end}$ are two constants for *c2*'s initial and final value

Simulation results with higher penetration level of PHEVs

For this simulation, the amount of signed PHEVs raise from 10 to 20. All the other generation data remains the same. The objective is to minimize the system daily operational cost, *C*, of this microgrid via particle swarm method stated in above.

With the growing amount of PHEVs, the V2G generation is expected to play a more and more important role in distributed generation. In Fig 6.26, the output from V2G increases greatly and occupies more percentage among all the DGs' outputs.

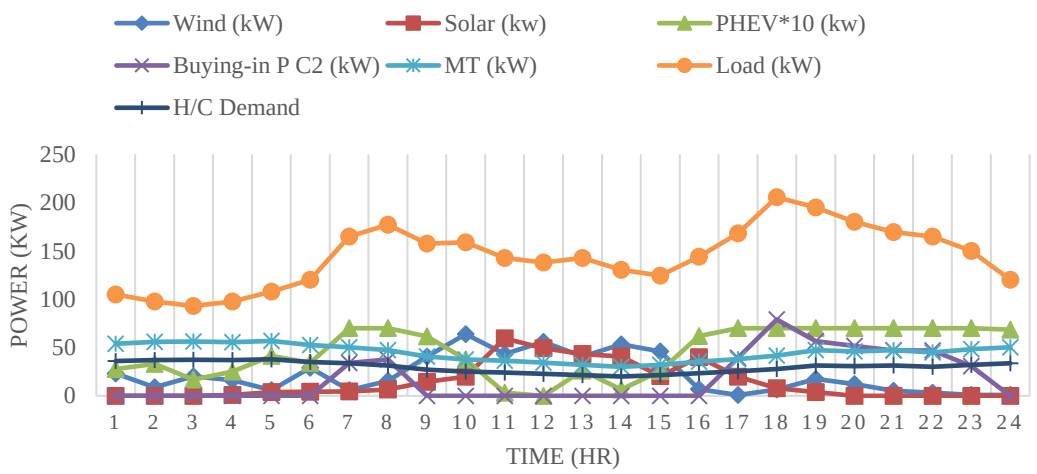

Figure 40 Generation from all power sources w higher penetration level

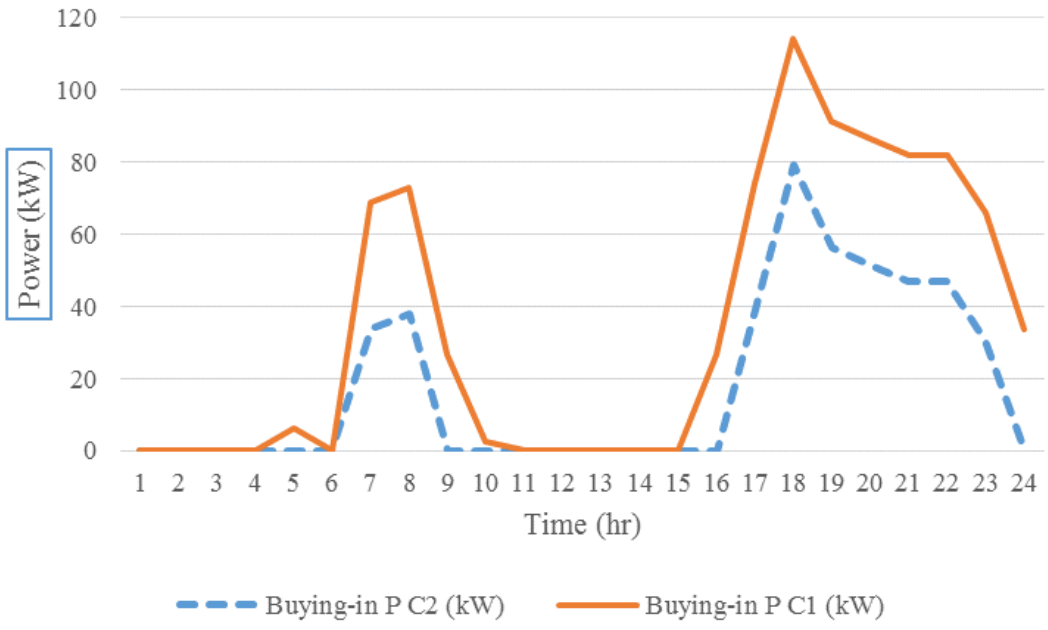

Figure 41 Buying-in power in both cases

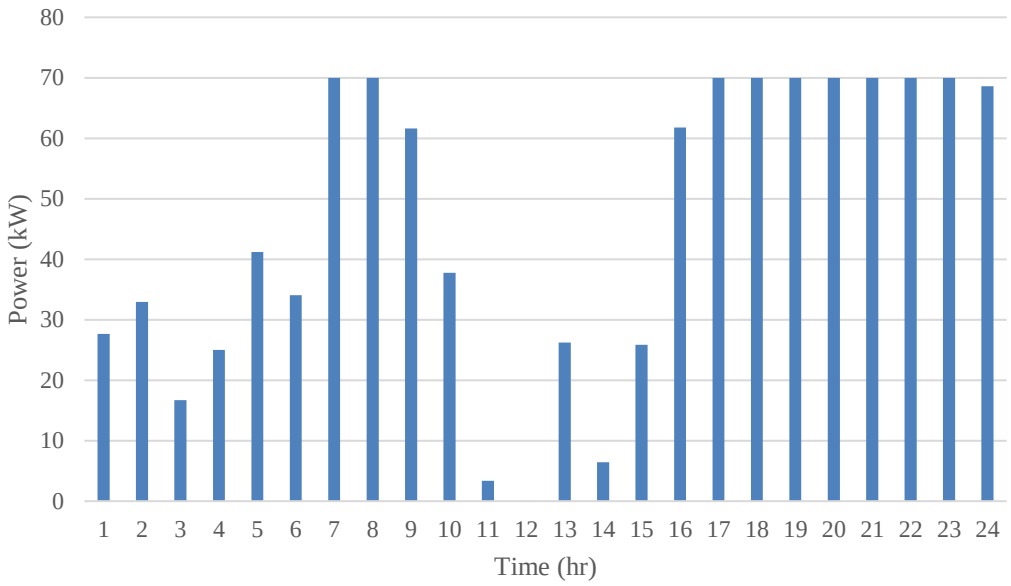

Figure 42 PHEV V2G output

In Figure 41, it is clear that the buying-in electricity from power grid or nearby microgrid decreases enormously. That means microgrid is more and more independent of the external grid. Meanwhile, the generation capacity and average output via V2G both increases due to the growing amount of PHEVs. With the generation from V2G becoming more and more reliable, the stability voltage and frequency in the microgrid can be improved with a higher penetration level of PHEVs.

Chapter 8. Optimization in Game theory

8.1 Game Theory Introduction

Electric storage units are inherently devices that can store energy, or extra electricity available at participating customers. Deployment of storage unit in future smart grid faces many challenges such as

1. Determining the required grid infrastructure (communication and control nodes) to enable smart energy exchange.

2. developing new power manage management strategies. Especially, with the penetration of PHEV loads.

3. The potential economic impact of deploying new types of energy storage devices, such as V2G.

The challenged that going to be discussed in this chapter is the analysis of the energy trading decision making processes involving complex interactions between the storage units and the various smart grid elements.

A game theoretic approach to the control of individual sources/loads was adopted to enhance the reliability and robustness of a power system without using central control. From the storage units' point of view, on the energy exchange market that arises due the competition among a number of storage , each of with could belong to a different customer and can interact at different levels. Due to the promising outlook of introducing energy storage units into the smart grid, devising new schemes to model and analyze the competition accompanying such energy exchange markets is both challenging and profitable.

In the following sections, a new frame work that enables a number of storage units belonging to different customers to individually and strategically choose the amount of stored energy that they wish to sell to customers in need of energy is developed. First of all, a double-auction market model is designed to allow the incorporation of power markets with multiple buyers and multiple sellers. Secondly, sellers are allowed to strategically decide on the amounts they put up for sale depending on the current market state. Thirdly, results are based on the existence of a Nash equilibrium. Last but not least, a learning algorithm is introduced to guarantee an equilibrium is reached for both market based auction and no cooperative game.

To achieve this innovative frame work, following two factors need to be addressed first.

1. Introducing a new approach using which the storage units can intelligently decide on the energy amount to sell while taking into account the effect of these decisions on both their utilities and the energy trading price in the market.

2. Developing and analyzing a mechanism to characterize the trading price of the energy trading market that involves the storage units and the potential energy buyers in the grid.

8.2 Power Market Modelling in Game Theory

In regulated market, the system operator is capable of conducting the optimized strategy that stated above. In previous simulation case, to dispatch the load demand and achieve the optimized result (Minimum generation cost), the system operator must have the "common knowledge" of the system and is "rational" to set up the strategy for all the micro energy sources. "Common knowledge" means the operator is informative of all the generation, transmission, and distribution data in the microgrid. In last case, being "rational" means the operator selects strategy depends on the total generation cost. For example, a rational operator always chooses the strategy with lower cost regardless of which energy sources are included in this strategy.

Since the generation data from the solar, wind, and PHEVs are all stochastic based, the system operator can evaluate and determine the optimal strategy based on the expected cost. This optimal strategy can be calculate through the procedure stated in

Chapter 7 every single time. However, if the simulation objective is a deregulated microgrid, every micro energy source can be treated as an energy seller. For each energy seller, they are also rational and have the common knowledge of the system. They know the outcome and payoff for their individual strategy as well. In this case, for each seller or player, the objective is to make more money in the energy trading market. Then, this energy trading in microgrid can be modelled as a no-cooperative game including sellers (utility) and buyers (demand).

For simplicity and comparison reason, the noncooperative game is applied to the previous IEEE 33-bus system microgrid system. The microgrid system contains N sellers and M buyer. ($N = 5$, $M = 3$). Each buyer $j \in M$ has a reservation bid b_j in the market indicating the price that she is willing to purchase the energy. The amount of energy demand over an hour is noted as d_j. d_j is the average value that the buyer expected to demand in one hour.

Each seller $i \in N$ is capable of choosing the amount of energy, s_i, which is willing to put into the market. s_i must satisfy following inequality.

$$s_i \leq C_i - R_i \quad (57)$$

C_i is the capacity of the energy storage utility i. R_i is the reservation amount of the energy storage utility i. Each seller i participate the energy trading market with a

reservation price, rp_i, for per unit energy. The reservation price indicate the lowest price that the player consider to sell the energy.

A no-cooperative normal-form game Γ is formulated to simulate the energy trading in microgrid includes three components as follows:

1. A finite set of players, $N = \{1, 2, 3, 4, 5\}$
2. A collection of pure strategies, $\{S_1, S_2, S_3, S_4, S_5\}$
3. A set of payoff functions, $\{v_1, v_2, v_3, v_4, v_5\}$

1) The five players are wind, solar, conventional plant 1, 2, and PHEVs. 2) The strategies for each player is the amount energy s_i that will be sold in the market. 3) The payoff function for each seller i is v_i which includes the revenue and cost with respect to the pure strategies s_i.

$$v_i(s_i, \mathbf{s}_{-i}) = \sum_{j \in M} \left[p_{ij}(\mathbf{s}) - rp_i \right] q_{ij}(\mathbf{s}) - f\left(\sum_{j \in M} q_{ij}(\mathbf{s}) \right) \quad (58)$$

In this payoff function, $\mathbf{s}_{-i}$ is a (N-1)*1 vector which includes all the strategies except utility i. $p_{ij}(\mathbf{s})$ is the trading price between seller i and buyer j. $q_{ij}(\mathbf{s})$ is the quantity of energy trading between seller i and buyer j. Function f() is the cost function of utility i. It mainly depends on two factors 1) type of energy source, 2) the total amount of sold energy $\sum q_{ij}(\mathbf{a})$. Generally, utility functions are defined for each type of energy source.

Moreover, utility function must be an increasing function with respect to the amount of sold energy.

In this no-cooperative energy trading game Γ, the objective of each seller is to take the best response by evaluating its own payoff function. In payoff function, the trading price $p_{ij}(\mathbf{s})$ has not been addressed yet. The trading price is a function of an N*1 strategy vector **s**. In this chapter, double auction mechanism is introduced to determine trading price in this energy market for each trade.

Double auction is a convenient method to obtain the trading price $p_{ij}(\mathbf{s})$, the amount of trading energy q, and the seller i and buyer j that participates in this trade. To begin with, the reservation prices, rp_i, are sorted in increasing order.

$$rp_1 < rp_2 < \cdots < rp_N \quad (59)$$

On the other hand, the biding prices, b_j, are sorted in decreasing order.

$$b_1 > b_2 > \cdots > b_M \quad (60)$$

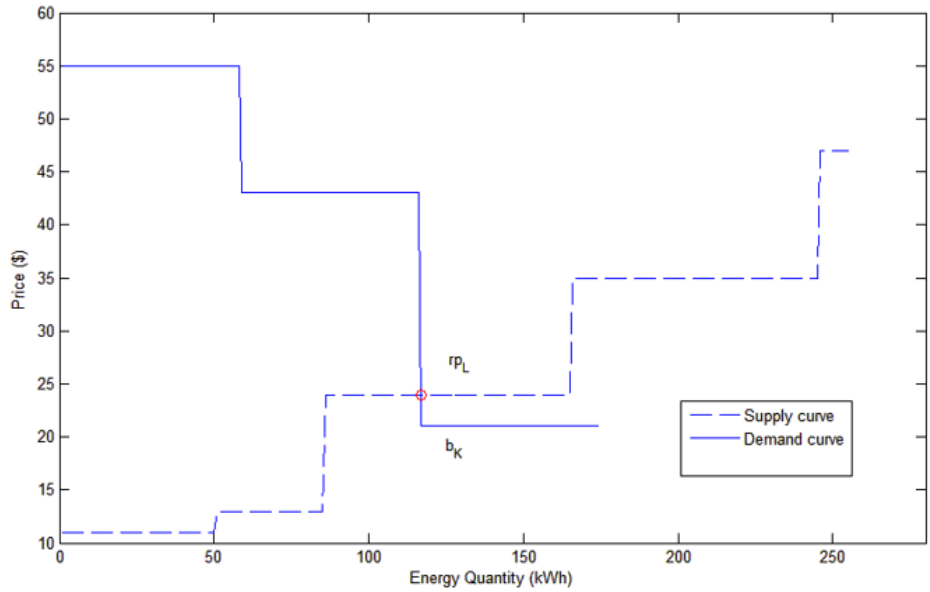

Figure 43 double auction market example

The reservation price sequence, rp_i, is used to generate the supply curve as a function of s_i (the amount of energy seller put into market). Similarly, the demand curve is generated by the buyer's bid, b_j, as a function of d_j (the amount of energy buyer demands). In most cases, these two curves intersects at a point. One double auction market example is shown in Figure 43. From this point, the first couple of seller L and buyer K can be easily traced to satisfy

$$b_K \geq rp_L \quad (61)$$

Then seller L -1 and buyer K -1 can follow up to participate the market and finish the energy trade.In the end, the total amount of supply and demand must match to

complete the energy trading process in an hour. According to the double auction method in [27][28], the trading price for seller $i < L$ and buyer $j < K$ can be any price that between rp_L and b_K. In this chapter, for simplicity, a unified trading price, $\bar{p}(\boldsymbol{s})$, is defined for all seller $i < L$ and buyer $j < K$.

$$\bar{p}(\mathbf{s}) = \frac{rp_L + b_K}{2} \quad (62)$$

The unified trading price is a function of vector **s** which means the trading price is depending on the individual seller's strategy $\{s_1, s_2, .., s_N\}$. The change of each seller's strategy can affect the intersection point of supply and demand curve. Consequently, the unified trading price can be different value as well.

Since the trading price has been determined, the amount of energy trading between seller $i < L$ and buyer $j < K$ need to be find out. A unified trading price $\bar{p}(\boldsymbol{s})$ is set up, as a result, for buyer $j < K$, only the amount of energy that put on sale differs the seller $i < L$. In addition, the cost function f() is defined as a quadratic function. Hence wise, the utility function becomes

$$v_i(s_i, \mathbf{s}_{-i}) = \left[\bar{p}(\mathbf{s}) - rp_i \right] Q_i(\mathbf{s}) - \alpha_i Q_i^2(\mathbf{s}) \quad (63)$$

α_i is the weighting factor depending on the type of energy source. $Q_i(\mathbf{s})$ is the total amount of energy that sold by seller i. The value is determined by below equation for a given strategy vector $\mathbf{s}$.

$$Q_i(\mathbf{s}) = \begin{cases} s_i & \sum_{j=1}^{K-1} d_j \geq \sum_{i=1}^{L-1} s_i \\ \max(0, s_i - \beta_i) & \sum_{j=1}^{K-1} d_j \leq \sum_{i=1}^{L-1} s_i \end{cases} \quad (64)$$

The function simply describes two scenarios. The first row is the over-demand scenario. The total demand for buyers $j < K$ is greater than the total supply for sellers $i < L$. As a rational seller, the strategy must be selling all the energy that plan to put into market.

On the other hand, in the oversupply scenario, the oversupply needs to be shared by the sellers $i < L$. Hence, the shared burden for seller i is

$$\beta_i = \frac{\sum_{i=1}^{L-1} s_i - \sum_{j=1}^{K-1} d_j}{L-1} \quad (65)$$

Iteratively, the remaining oversupply burden is shared by the left L-2 sellers till all the utility sells a non-negative value.

Based on the double auction method that stated above, each seller i is capable to set up the strategy (s_i, amount of energy to sell). The objective is always to maximize its own payoff considering all the other sellers' strategies. Among different kinds of methods (IESDS, rationalizability, etc.), Nash equilibrium (NE) is selected to find out the most possible solution for a rational and knowledgeable seller. The definition of Nash equilibrium is

The pure strategy profile $s^* = (s_1^*, s_2^*, \dots, s_n^*) \in S$ is a Nash equilibrium if s_i^* is a best response to s_{-i}^*, for all $i \in N$, that is

$$v_i(s_i^*, s_{-i}^*) \geq v_i(s_i^{'}, s_{-i}^*) \quad \text{for all } s_i^{'} \in S_i \text{ and all } i \in N \quad (66)$$

However, it is not guaranteed that for every game the Nash equilibrium must exist. As a result, before apply the NE method, the existence of NE in the noncooperative double auction game must be proven first. According to [29], the following theorem is introduced.

For the noncooperative game Γ, at least one pure-strategy Nash equilibrium exists. The detailed proven can also be found in [29]. Since the NE exists, to find out the NE, the best response of each seller must be defined first.

The strategy $s_i \in S_i$ is player i's best response to his opponents' strategies $s_{-i} \in S_{-i}$ if

$$v_i(s_i, s_{-i}) \geq v_i(s_i^{'}, s_{-i}) \quad \forall s_i^{'} \in S_i \quad (67)$$

Each seller (player) always set up the strategy to maximize its own payoff as the best response to his beliefs of the opponents' strategies. Another requirement for a NE is that his beliefs of the players about their opponents are correct. The common solution or solutions within the best responses from all the players is or are the Nash Equilibria solution(s). Following iterative algorithm [30] is introduced to ensure the game converge to a Nash Equilibria solution.

$$s_i^{(n+1)} = (1-\omega) r\left(\mathbf{s}_{-i}^{(n)}\right) + \omega s_i^{(n)} \quad (68)$$

$$\begin{aligned} r(\mathbf{s}_{-i}) &= \arg\max\left[v_i(s_i, \mathbf{s}_{-i})\right] \\ &= \left\{\left[\overline{p}(\mathbf{s}) - rp_i\right] Q_i(\mathbf{s}) - \alpha_i Q_i^2(\mathbf{s})\right\} \\ &= \begin{cases} \dfrac{\overline{p}(\mathbf{s}) - rp_i}{2\alpha_i} & \sum_{j=1}^{K-1} d_j \geq \sum_{i=1}^{L-1} s_i \\ \dfrac{\left[\overline{p}(\mathbf{s}) - rp_i\right](L-1) + 2\alpha_i\left(\sum_{i=1}^{L-1} s_i - \sum_{j=1}^{K-1} d_j\right)}{2\alpha_i (L-1)} & \sum_{j=1}^{K-1} d_j \leq \sum_{i=1}^{L-1} s_i \end{cases} \end{aligned} \quad (69)$$

ω is a searching inertia weight, $0 < \omega < 1$. The converge criterion is $\left|s_i^{(n+1)} - s_i^n\right| < \varepsilon$. After a number of iteration, the s_i will converge and the final iteration is shown below. The final Nash equilibria solution s_i is obtained for seller *i*.

$$(1-\omega)s_i^{(F+1)} = (1-\omega)r\left(s_{-i}^{(F)}\right)$$
$$s_i^{(F+1)} = r\left(s_{-i}^{(F)}\right) \quad (70)$$

8.3 Case study – Noncooperative Energy Trading Game in 33-bus Microgrid System.

To apply the iterative algorithm to the microgrid case, firstly, each player needs to set an initial value of their strategy. In microgrid case, seller *i* will decide how much energy, s_i, they are willing put into the market. To ensure the total supply and demand can match, the initial strategy of each seller is assumed as the maximum surplus energy which is available for sale.

$$s_i^{\text{int}} = C_i - R_i \quad \forall i \in N \quad (71)$$

Then, the iterative process begins with all the initial values. After each iteration, each seller adjust his strategy to obtain a better payoff as a response to his opponents' strategies. In the final iteration, all the seller reaches his best response. Consequently, the noncooperative game also reaches its Nash equilibrium. In this microgrid case, the sellers (micro energy source utilities) are assumed to act in a set order. After the strategy phase, the sellers put the amount of energy which is suggested as the best response into the energy trading market for rewards accordingly.

In actual simulation, the search inertia weight, ω, affects the computation efficiency. The criterions to evaluate ω is 1) the result of NE convergence 2) the number of iteration it takes to converge. To find the optimized search inertia, since the interval is from 0 to 1, the simplest method is to arbitrarily start from 1 and decrease in a small interval (e.g. 0.1) to dig out the solution. Obviously, the method must work but also takes a great amount time. To improve the efficiency, two methods from optimization can be introduced. One is the bisection method. Another is the gold section method. Bisection method use the mid-point to narrow down the interval of searching in each iteration. Gold section method use gold section point instead of mid-point. In following part, gold section method is utilized to calculate the optimized searching inertia weight, ω.

Table 15 Parameters of micro energy sources

	Surplus energy (kWh)	Cost weighting factor α ($/kWh^2)
Wind	50	0.2
Solar	35	0.2
CPP1	80	0.1
CPP2	80	0.12
PHEV*35	10	1

Surplus energy and cost weighting factor α is shown in above table. The reservation price for each seller is randomly generated from a range of [10, 50] dollars per MWh. Similarly, the price bid for each buyer is randomly chosen from a range of [15, 60] dollars per MWh. Via gold section method, Searching inertia weight, ω, is calculated to be 0.45.

Firstly, four scenarios is applied to the model to test the performance of the double auction energy trading market. They are low demand (100 kWh), medium demand (300 kWh), high demand (500 kWh), and peak demand (700 kWh). The supply and demand curves and intersection points are show in Figure 44.

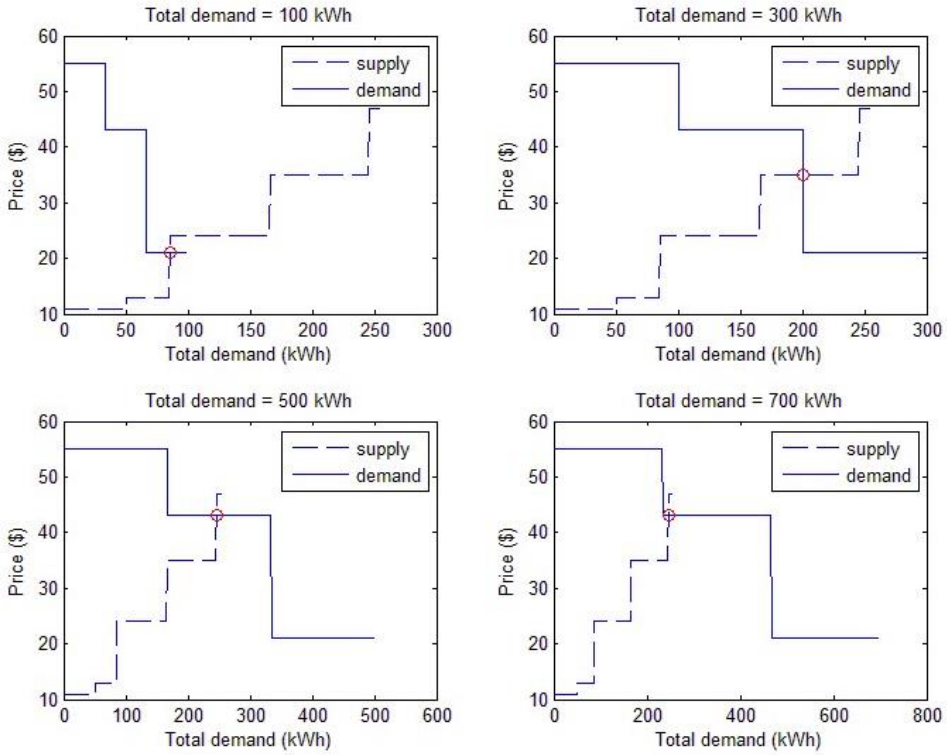

Figure 44 Double auction model in four scenarios (100, 300, 500, and 700 kWh)

From the simulation result, it is clear that the double auction market acts similar to the actual real-life market in trading price aspect. The higher the demand from all the sellers always result in a higher unified trading price. The increasing trend is illustrated in Figure 45. The price increases from $21 (100 kWh case) to $43 (500 and 700 kWh cases). From amount of trading energy aspect, the higher demand results in the more trading energy after double auction. Consequently, more trading energy means more

sellers can participate in market and complete energy trading. Especially for V2G, due to the highest generation cost, V2G is only capable of picking up the peak load if necessary.

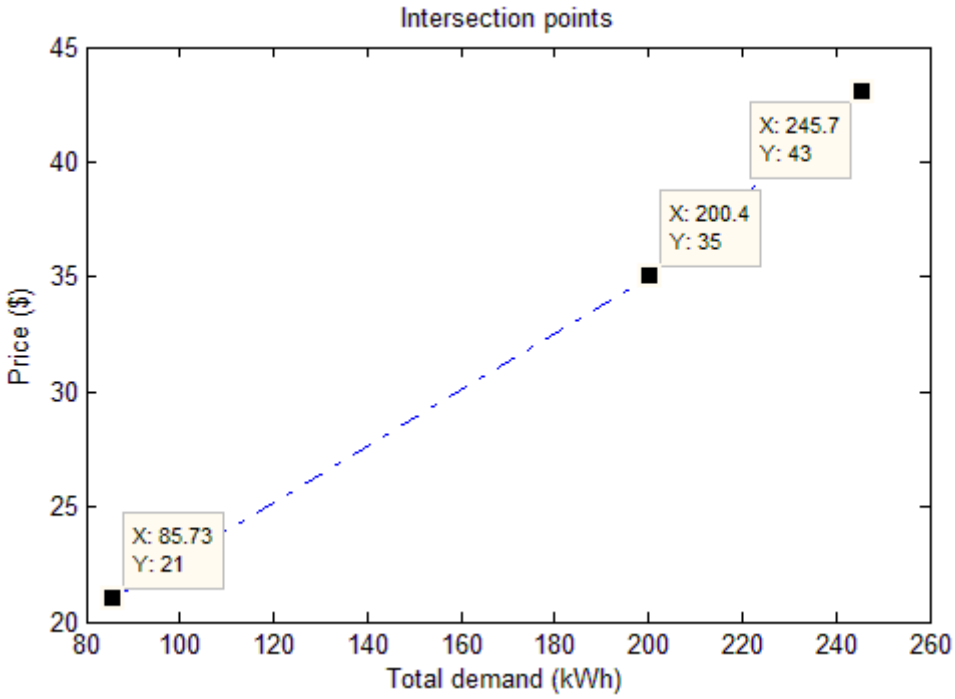

Figure 45 Intersection points in four scenarios (100, 300, 500, and 700 kWh)

In following case, the total demand is set as 175 kWh. Buyer 1, 2, and 3 share the demand evenly. To search for the Nash equilibrium, the iterative method stated in 8.2 is utilized. The detailed procedure is listed below.

1. From initial strategy s_i^{int} to get unified price $\bar{p}(\mathbf{s})$ (Maximum capacity for each seller)
2. Apply $\bar{p}(\mathbf{s})$ in the utility function to approach the best response $r(\mathbf{s}_{-i})$

3. Update the strategy $\mathbf{s}_i$ and repeat step 1 and 2 till the result converge to Nash equilibrium.

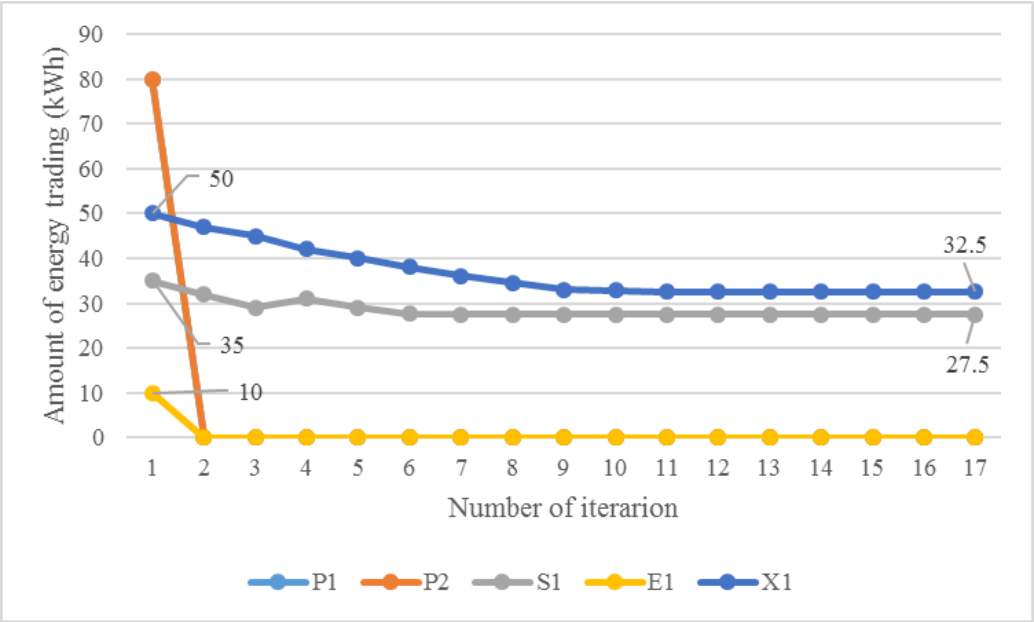

Figure 46 Nash Equilibrium via iterative method

In Figure 46, after 17 iterations, the converged result show that only wind (X1) and solar (S1) will participate and complete trading. The amount of energy trading of other three micro energy sources (P1, P2, and E1) drops to zero in second iteration which means that they are not competitive in this scenario (demand = 175 kWh) and their best response is to remain idle and sell no energy.

Simulation result analysis

- Computational complexity is challenging due to the fact that the trading price varies during the iterative process. The computational complexity of compare

supply and demand curves and find the intersection point is O (L + K), since the unified price is determined by seller L and buyer K. In overdemand condition, the best response, $r(\boldsymbol{s}_{-i}) = \frac{\bar{p}(\boldsymbol{s}) - rp_i}{2\alpha_i}$, is independent of market size. So, the computational complexity is O(1). On the other hand, if supply is greater and demand, the best response, $r(\boldsymbol{s}_{-i}) = \frac{[\bar{p}(\boldsymbol{s}) - rp_i](L-1) + 2\alpha_i\left(\sum_{i=1}^{L-1} s_i - \sum_{j=1}^{K-1} d_j\right)}{2\alpha_i(L-1)}$, is depend on seller L and buyer K. The computational complexity is also O (L + K). In this case study, only L -1 sellers' best responses are considered. K – 1 buyers are assumed to hold and do no change their strategies. Since the sequential algorithm is utilized in above case, the computational complexity then is O (L - 1) (L + K).

$$r(\mathbf{s}_{-i}) = \begin{cases} \dfrac{\bar{p}(\mathbf{s}) - rp_i}{2\alpha_i} & \sum_{j=1}^{K-1} d_j \geq \sum_{i=1}^{L-1} s_i \\ \dfrac{\left[\bar{p}(\mathbf{s}) - rp_i\right](L-1) + 2\alpha_i\left(\sum_{i=1}^{L-1} s_i - \sum_{j=1}^{K-1} d_j\right)}{2\alpha_i(L-1)} & \sum_{j=1}^{K-1} d_j \leq \sum_{i=1}^{L-1} s_i \end{cases} \quad (72)$$

- PHEV V2G approach is not competitive in energy trading market comparing to the microgrid optimization case. V2G supplies energy in 18:00, 19:00, 20:00, and 23:00 in microgrid case. In comparison, V2G is in service only in peak demand in double auction market.
- Nash equilibrium in most scenarios is not the Pareto optimal can result in waste of social resources. A system operator who is informative of the data from transmission distribution system and energy sources in microgrid is capable of

optimizing the economic dispatch and utilizing the preferred energy sources (wind, solar).

Chapter 9. Research Conclusion and Future Work

With the growth of the amount of PHEVs, the implementation of V2G method with large scale renewable energy will be the next inevitable challenge for current power system [31]-[34]. If V2G and renewable energy are not coordinated, the charging loads of PHEVs would surely present a great pressure on the distribution level grid [35]-[40].

In this dissertation, a stochastic forecasting model is developed for PHEV charging load. Based on the prediction data, the Loss of Life of distribution transformer can be a burden for current distribution system. Particle swarm optimization method is applied to relieve the pressure on distribution transformer. The simulation results reveal that without replacing existing distribution transformer the pressure can be greatly reduced by re-scheduling the PHEV charging plan.

For charging strategy optimization in microgrid, a versatile distribution model is utilized to forecast the output error for wind farm, V2G, and solar farm. Then, the probabilistic distribution models are applied to economic dispatch problem in microgrid. From the modified IEEE 33 Bus case study results, it reveals that V2G can serve as a quick responsive energy source to accommodate peak loads. As a result, the power quality in microgrid can be improved. Furthermore, simulation is also conducted in deregulated energy market in the same modified IEEE 33 bus system. The energy trading market is considered as a noncooperative normal game with energy sellers and buyers. The simulation results reveal that V2G is not a favorable micro energy source in deregulated market expect the peak demand period.

In conclusion, transportation electrification in both regular distribution system and microgrid will surely play a more and more important role. If proper optimization strategy is applied, the negative impact of high penetration level of PHEVs' charging load can be minimized. Moreover, since the main energy sources in microgrid are wind and solar farms in future, the microgrid system always needs a reliable and responsive power source. V2G can be a favorable option with the increasing penetration level of PHEVs. On the other hand, V2G is able to help microgrid become more independent of external power grid.

References

[1] Wencong Su, Mo-Yuen Chow, "Performance Evaluation of A PHEV Parking Station Using Particle Swarm Optimization," IEEE Power and Energy Society General Meeting, 2011.

[2] Yingzhong Gu, Le Xie, "Look-ahead Coordination of Wind Energy and Electric Vehicles: A Market-based Approach," North American Power Symposium (NAPS), 2010.

[3] K.J. Yunus, M. Reza, H. Zelaya-De La Parra, K. Srivastava, "Impacts of Stochastic Residential Plug-In Electric Vehicle Charging on Distribution Grid," IEEE PES Innovative Smart Grid Technologies (ISGT), 2012.

[4] Zhuowei Luo, Yonghua Song, Zechun Hu, Zhiwei Xu, Xia Yang, Kaiqiao Zhan, "Forecasting Charging Load of Plug-in Electric Vehicles in China," IEEE Power and Energy Society General Meeting, 2011.

[5] Wencong Su, Mo-Yuen Chow, "Computational Intelligence-based Energy Management for a Large-scale PHEV/PEV Enabled Municipal Parking Deck," Applied Energy, Volume 96, August 2012, Pages 171-182, Smart Grids.

[6] L. Lazic, G. Pejanovic, and M. Zivkovic, "Wind forecasts for wind power generation using the Eta model," Renewable Energy, vol. 35, no. 6, pp. 1236-1243, June 2010.

[7] J. Tambke, et al., "Short-term Forecasting of Offshore Wind Farms Production –Developments of the Anemos Project". In Proc. of the European Wind Energy Conference 2006, Athens, Greece, 27/2-2/3 2006.

[8] Research and Innovation Technology Administration Bureau of Transportation Statistics [Online]. Available: http://www.bts.gov/publications/highlights_of_the_2001_national_household_travel_survey/html/section_02.html

[9] G. Giebel, G. Kariniotakis, and R. Brownsword, "The State-of-the-Art in Short-Term Prediction of Wind Power - Aliterature Review,[Online]: Available: http: //www.anemos-project.eu/download//ANEMOS_D1.1_StateOfTheArt_v1.1.pdf.

[10] A. R. Garcia, and E. De-La-Torre-Vega, "A Statistical wind power forecasting system – A Mexican wind-farm case study," European Wind Energy Conference & Exhibition – EWEC Parc Chanot, Marseille, France, March 2009.

[11] Chicago Transit Authority, http://www.transitchicago.com/about/facts.aspx

[12] BYD electric bus parameters, http://www.byd.com/ElectricBus.htm

[13] Columbia university's school of international and public affairs and the earth institute, master of public administration program in environmental science and policy, workshop in applied earth system policy analysis, final workshop report.

[14] BYDe6 parameters, www.byd.com/e6.html

[15] http://www.plugincars.com/2012-plug-sales-already-flop-111651.html

[16] http://www.howmanyarethere.org/how-many-cars-are-there-in-the-usa-2012/

[17] Bharadwaj Ranganathan Sathyanarayana, “The effect of ambient temperature rise on distribution transformer service life”, Master Thesis, Arizona State University, Oct. 2008.

[18] RELOAD Database Documentation and Evaluation and Use in NEMS [Online]. Available: http://www.onlocationinc.com/LoadShapesReload2001.pdf

[19] Zhao-Sui Zhang, Yuan-Zhang Sun, David Wenzhong Gao, Jin Lin, and Lin Cheng, “A Versatile Probability Distribution Model for Wind Power Forecast Errors and Its Application in Economic Dispatch,” IEEE Transactions on Power Systems, Vol. 28, No. 3, 2013.

[20] John Hetzer, David C. Yu, and Kalu Bhattarai, “An Economic Dispatch Model Incorporating Wind Power,” IEEE Transactions on Energy Conversion, Vol. 23, No. 2, June 2008.

[21] Solar farm data, http://sites.google.com/site/luisfochoa/research/opendss-training

[22] Ziqiao Liu, Wenzhong Gao, Yih-hui Wan, Eduard Muljadi, "Wind Plant Power Prediction by Using Neural Network Methods," the 4th IEEE Energy Conversion Congress and Exposition, Raleigh, North Carolina, September 16-20, 2012.

[23] Yin Yao, Wenzhong Gao, Yan Li, “Optimization of PHEV Charging Schedule for Load Peak Shaving,” IEEE Conference and Expo on Transportation Electrification Asia-Pacific (ITEC Asia-Pacific), 2014.

[24] Yin Yao, Wenzhong Gao, “Relieving the Pressure of Electric Vehicle Battery Charging on Distribution Transformer via Particle Swarm Optimization Method,” North American Power Symposium (NAPS), 2014.

[25] S. Mishra, Y. Mishra, and S. Vignesh, “Security constrained economic dispatch considering wind energy conversion system,” in Proc. IEEE Power and Energy Society General Meeting, Detroit, MI, USA, 2011.

[26] Katsuhisa Yoshimoto, Toshiya, Gentaro Koshimizu and Yoshihsa Uchida, “New control method for Regulating state-charge of a battery in hybrid wind power/battery energy storage system,” in Proc. Int. Conf. PSCE, 2006, pp.1244-1251.

[27] D. Friedman, D. P. Friedman, and J. Rust, The Double Auction Market: Institutions, Theories, and Evidence. Boulder, CO, USA: Westview Press, 1993.

[28] P. Huang, A. Scheller-Wolf, and K. Sycara, “Design of a multi-unit double auction e-market,” Comput. Intell., vol. 18, no. 4, pp: 596-617, Feb. 2002.

[29] P. Dasgupta and E. Maskin, “The existence of equilibrium in discontinuous economic games, I: Theory,” JSTOR Rev. Econ. Studies, vol. 53, no. 1, pp. 1-26, Jan. 1986.

[30] Yunpeng Wang, Walid Saad, Zhu Han, H. Vincent Poor, and Tamer Basar, “A Game-Theoretic Approach to Energy Trading in the Smart Grid,” IEEE Transactions on Smart Grid, Vol. 5, No. 3, May 2014.

[31] W. Kempton, J. Tomic, “Vehicle-to-grid power implementation: from stabilizing the grid to supporting large-scale renewable energy,” Journal of Power Sources, Vol. 144, No. 1, June 2005.

[32] Jayakrishnan Radhakrishna Pillai, Birgitte Bak-Jensen, “Integration of Vehicle-to-Gird in the Western Danish Power System,” IEEE Trans. Sustainable Energy, vol. 2, no. 1, pp. 12-19, 2001.

[33] John Patten, Nathan Christensen, Gary Nola, Steven Srivastava, “Electric Vehicle Battery – Wind Storage System,” IEEE Vehicle Power and Propulsion Conference (VPPC), 2011.

[34] Christophe Guille, George Gross, “The Integration of PHEV Aggregations into a Power System with Wind Resources,” Bulk Power System Dynamics and Control (iREP) – VIII (iREP), 2010.

[35] Y. W. Li and C.-N. Kao, “An accurate power control strategy for power electronics-interfaced distributed generation units operating in a low-voltage multibus microgrid,” IEEE Transactions on Power Electronics, Vol. 24, No. 12, 2009.

[36] Shengnan Shao, Manisa Pipattanasomporn, Saifur Rahman, “Challenges of PHEV Penetration to the Residential Distribution Network,” IEEE Power & Energy Society General Meeting, 2009.

[37] Eric Sortomme, Mohammad M. Hindi, S. D. James MacPherson, S. S. Venkata, “Coordinated Charging of Plug-In Hybrid Electric Vehicles to Minimize Distribution System Losses,” IEEE Trans. Smart Grid, vol. 2, no. 1, pp. 198-205, 2011.

[38] Zhi Zhou, Jianhui Wang, Audun Botterud, “Agent-based Electricity Market Simulation with Plug-in Hybrid Electric Vehicle Penetration,” IEEE Power and Energy Society General Meeting, 2011.

[39] Seshadri Srinivasa Raghavan, Alireza Khaligh, “Impact of Plug-in Hybrid Electric Vehicle Charging on a Distribution Network in a Smart Grid Environment,” IEEE Innovative Smart Grid Technologies (ISGT), 2012.

[40] Jad Mouawad and Kate Galbraith (2009-12-14), “Study Says Big Impact of the Plug-in Hybrid Will be Decades away,” New York Times, Retrieved 2010-03-04

[41] Olimpo Anaya-Lara, Nick Jenkins, Janaka Ekanayake, Phill Cartwright, and Mika Hughes, "Wind Energy Generation Modeling and Control," Library of Congress Cataloguing-in-Publication Data, 1st Edition. United Kingdom, Wiley, 2009.

[42] Bredan Fox, Damian Flynnm Leslie Bryans, Nick Jenkins, David Milborrowm, Mark O’Malley, Richard Watsn, and Olimp Anaya-Lara, "Wind Power Integration, " IET Power and Energy Series 50, The Institution of Engineering and Technology, 1st Edition, London, United Kingdom 2007.

[43] Jain, Pramod. Wind energy engineering. McGraw-Hill, 2011.

[44] Milovanþeviü, Miloš, and Boban Anÿelkoviü. "MODERN TECHNIQUES OF WIND TURBINE CONDITION MONITORING."

[45] Sheng, S., H. Link, W. LaCava, J. van Dam, B. McNiff, P. Veers, J. Keller, S. Butterfield, and F. Oyague. "Wind turbine drivetrain condition monitoring during GRC Phase 1 and Phase 2 testing." Contract 303 (2011): 275-3000.

[46] Li, Yanyong. "Discussion on the principles of wind turbine condition monitoring system." In Materials for Renewable Energy & Environment (ICMREE), 2011 International Conference on, vol. 1, pp. 621-624. IEEE, 2011.

[47] García Márquez, Fausto Pedro, Andrew Mark Tobias, Jesús María Pinar Pérez, and Mayorkinos Papaelias. "Condition monitoring of wind turbines: Techniques and methods." Renewable Energy 46 (2012): 169-178.

[48] Hyers, R. W., J. G. McGowan, K. L. Sullivan, J. F. Manwell, and B. C. Syrett. "Condition monitoring and prognosis of utility scale wind turbines." Energy Materials: Materials Science and Engineering for Energy Systems 1, no. 3 (2006): 187-203.

[49] Ackermann, Thomas, ed. Wind power in power systems. Vol. 140. Chichester, UK: John Wiley, 2005.

[50] Entezami, Mani, Stuart Hillmansen, and Clive Roberts. "Wind Turbine Condition Monitoring System." PhD Progress Report, University of Birmingham (2010).

[51] Verbruggen, T. W. Wind Turbine Operation & Maintenance based on Condition Monitoring WT-Ω. April, 2003.

[52] Laakso, Kari, Tony Rosqvist, and Jette L. Paulsen. The use of condition monitoring information for maintenance planning and decision-making. Technical Report. NKS-80, 2002.

[53] Alewine, Kevin, and William Chen. "A review of electrical winding failures in wind turbine generators." In Electrical Insulation Conference (EIC), 2011, pp. 392-397. IEEE, 2011.

[54] Lu, Bin, Yaoyu Li, Xin Wu, and Zhongzhou Yang. "A review of recent advances in wind turbine condition monitoring and fault diagnosis." In Power Electronics and Machines in Wind Applications, 2009. PEMWA 2009. IEEE, pp. 1-7. IEEE, 2009.

[55] Guo, Peng, David Infield, and Xiyun Yang. "Wind turbine generator condition-monitoring using temperature trend analysis." Sustainable Energy, IEEE Transactions on 3, no. 1 (2012): 124-133.

[56] Yang, Wenxian, P. J. Tavner, and Michael Wilkinson. "Condition monitoring and fault diagnosis of a wind turbine with a synchronous generator using wavelet transforms." In Power Electronics, Machines and Drives, 2008. PEMD 2008. 4th IET Conference on, pp. 6-10. IET, 2008.

[57] Watson, Simon Jonathan, Beth J. Xiang, Wenxian Yang, Peter J. Tavner, and Christopher J. Crabtree. "Condition monitoring of the power output of wind turbine generators using wavelets." Energy Conversion, IEEE Transactions on 25, no. 3 (2010): 715-721.

[58] Amirat, Yassine, Vincent Choqueuse, and Mohamed Benbouzid. "Wind turbine bearing failure detection using generator stator current homopolar component ensemble empirical mode decomposition." In IECON 2012-38th Annual Conference on IEEE Industrial Electronics Society, pp. 3937-3942. IEEE, 2012.

[59] Gong, Xiang, and Wei Qiao. "Bearing fault detection for direct-drive wind turbines via stator current spectrum analysis." In Energy Conversion Congress and Exposition (ECCE), 2011 IEEE, pp. 313-318. IEEE, 2011.

[60] Popa, Lucian Mihet, Birgitte-Bak Jensen, Ewen Ritchie, and Ion Boldea. "Condition monitoring of wind generators." In Industry Applications Conference, 2003. 38th IAS Annual Meeting. Conference Record of the, vol. 3, pp. 1839-1846. IEEE, 2003.

[61] Damian S. Vilchis-Rodriguez, Sinisa Djurovic, Alexander C. Smith, " Wind turbine induction generator bearing fault detection using stator current analysis, " IET Renewable Power Generation, Vol. 7, Iss. 4, pp. 330–340, 2013

[62] Yazidi, A., H. Henao, G. A. Capolino, D. Casadei, F. Filippetti, and C. Rossi. "Simulation of a doubly-fed induction machine for wind turbine generator fault analysis." In Diagnostics for Electric Machines, Power Electronics and Drives, 2005. SDEMPED 2005. 5th IEEE International Symposium on, pp. 1-6. IEEE, 2005.

[63] Han, Y., and Y. H. Song. "Condition monitoring techniques for electrical equipment-a literature survey." Power Delivery, IEEE Transactions on 18, no. 1 (2003): 4-13.

[64] Yang, Wenxian, Jiesheng Jiang, P. J. Tavner, and C. J. Crabtree. "Monitoring wind turbine condition by the approach of Empirical Mode Decomposition." In Electrical Machines and Systems, 2008. ICEMS 2008. International Conference on, pp. 736-740. IEEE, 2008.

[65] Yang, Wenxian, Peter J. Tavner, Christopher J. Crabtree, and Michael Wilkinson. "Cost-effective condition monitoring for wind turbines." Industrial Electronics, IEEE Transactions on 57, no. 1 (2010): 263-271.

[66] Tian, Zhigang, Tongdan Jin, Bairong Wu, and Fangfang Ding. "Condition based maintenance optimization for wind power generation systems under continuous monitoring." Renewable Energy 36, no. 5 (2011): 1502-1509.

[67] Avelino J. Gonzalez, M. Stanley Balowin, J. Stein, and N. E. Nilsson, "Monitoring and Diagnosis of Turbine-Driven Generator," Electric Power Research Institute, Prentice Hall, Englewood Cliffs, New Jersey 07632,1995

[68] Nandi, Subhasis, Seungdeog Choi, and Homayoun Meshgin-kelk. Electric Machines: Modeling, Condition Monitoring, and Fault Diagnosis. CRC Press, 2012.

[69] Yang, Wenxian, P. J. Tavner, and M. R. Wilkinson. "Condition monitoring and fault diagnosis of a wind turbine synchronous generator drive train." Renewable Power Generation, IET 3, no. 1 (2009): 1-11.

[70] Bang, D., H. Polinder, G. Shrestha, and J. A. Ferreira. "Review of generator systems for direct-drive wind turbines." In European Wind Energy Conference & Exhibition, Belgium, pp. 1-11. 2008.

[71] Peter Tavner, Li Ran, Jim Penman, and Howard Sedding, "Condition Monitoring of Rotating Electrical Machines," IET POWER AND ENERGY SERIES 56. Published by The Institution of Engineering and Technology, London, United Kingdom 2008.

[72] Lu, Wenxiu, and Fulei Chu. "Condition monitoring and fault diagnostics of wind turbines." In Prognostics and Health Management Conference, 2010. PHM'10. pp. 1-11. IEEE, 2010.

[73] Qiao, Wei, Ganesh K. Venayagamoorthy, and Ronald G. Harley. "Optimal wide-area monitoring and nonlinear adaptive coordinating neurocontrol of a power system with wind power integration and multiple FACTS devices." Neural Networks 21, no. 2 (2008): 466-475.

[74] Kusiak, Andrew, Haiyang Zheng, and Zhe Song. "Models for monitoring wind farm power." Renewable Energy 34, no. 3 (2009): 583-590.

[75] Giebel, Gregor, Oliver Gehrke, Malcolm McGugan, and Kaj Borum. "Common access to wind turbine data for condition monitoring the IEC 61400-25 family of standards." (2006): 157-164.

[76] Benbouzid, Mohamed El Hachemi, Michelle Vieira, and Céline Theys. "Induction motors' faults detection and localization using stator current advanced signal processing techniques." Power Electronics, IEEE Transactions on 14, no. 1 (1999): 14-22.

[77] Jung, Jee-Hoon, Jong-Jae Lee, and Bong-Hwan Kwon. "Online diagnosis of induction motors using MCSA." Industrial Electronics, IEEE Transactions on 53, no. 6 (2006): 1842-1852.

[78] Penman, J., M. N. Dey, A. J. Tait, and W. E. Bryan. "Condition monitoring of electrical drives." Electric Power Applications, IEE Proceedings B 133, no. 3 (1986): 142-148.

[79] Tavner, P. J., B. G. Gaydon, and D. M. Ward. "Monitoring generators and large motors." Electric Power Applications, IEE Proceedings B 133, no. 3 (1986): 169-180.

[80] Kiani, Morgan, and Wei-Jen Lee. "Effects of voltage unbalance and system harmonics on the performance of doubly fed induction wind generators." Industry Applications, IEEE Transactions on 46, no. 2 (2010): 562-568.

[81] Djurovic, S., S. Williamson, P. J. Tavner, and W. Yang. "Condition monitoring artefacts for detecting winding faults in wind turbine DFIGs." In Proc. EWEC, pp. 16-19. 2009.

[82] Kevin Alewine, "Wind Turbine Generator Failure Modes, "Renewable Energy Services. Shermco Industries, http://www.nrel.gov/wind/pdfs/day1_sessioniv 04_shermco_alewine.pdf.

[83] Hameed, Z., Y. S. Hong, Y. M. Cho, S. H. Ahn, and C. K. Song. "Condition monitoring and fault detection of wind turbines and related algorithms: A review." Renewable and Sustainable energy reviews 13, no. 1 (2009): 1-39.

[84] Douglas C. Montgomery, Elizabeth A. Peck, and Geoffrey Vining, "Introduction to Linear Regression Analysis," WILEY, Fifth edition 2012.

[85] Achinity Haldar, and Sankaran Mahadevan, "Probability, Reliability, and Statistical Method in Engineering Design," WILLY 2000.

[86] J. F. Manwell, J.G.Mcgowan, and A.L.Rogers, "Wind Energy Explained Theory, Design, and Application," WILLY, Second edition 2009.

[87] Incropera, DeWitt, Bergman, and Lavine, "Fundamentals of Heat and Mass Transfer," IET Renewable Power Generation, April 2008.

[88] John H. Lienhard IV, John H. Lienhard V, "Heat Transfer Textbook, Third Edition, 2008.

[89] Minitab 16 software, http://www.minitab.com

[90] IBM SPSS software, http://www-01.ibm.com/software/analytics/products/

[91] statistics/index.html

[92] Data of a variable speed wind turbine 450 KW rated power, three phase permanent magnetic type 440/660 V 60 Hz. Provided by Dr. Kathryn, Colorado School of Mines, 2013.

[93] Frank S. Barnes, and Jonah G. Levine, "Large Energy Storage System Handbook, "CRC Press, Taylor & Francis Group, 2011.

[94] Wilkinson, Michal R., Fabio Spinato, and Peter J. Tavner. "Condition monitoring of generators & other subassemblies in wind turbine drive trains." In Diagnostics for Electric Machines, Power Electronics and Drives, 2007. SDEMPED 2007. IEEE International Symposium on, pp. 388-392. IEEE, 2007.

[95] Data of a variable speed wind turbine 5 MW rated power, three phase permanent magnetic type 440/660 V 60 Hz. Provided by Dr. Kathryn, Colorado School of Mines, 2013.

[96] Preecha, P., and J. Dejvises. "The power losses calculation technique of electrical machines using the heat transfer theory." In Power Engineering Conference, 2007. IPEC 2007. International, pp. 297-301. IEEE, 2007.

[97] Ramesh K. Shah, Dušan P. Sekulić "Fundamental of Heat Exchanger Design," Published online, 2007.

[98] Yanyong Li, "Fluid Mechanices," Thennal Energy Dynamics Research Institute, IEEE, 2011.

[99] Amirat, Yassine, Mohamed El Hachemi Benbouzid, Elie Al-Ahmar, Bachir Bensaker, and Sylvie Turri. "A brief status on condition monitoring and fault diagnosis in wind energy conversion systems." Renewable and Sustainable Energy Reviews 13, no. 9 (2009): 2629-2636.

[100]Muljadi, E., and J. Green. "Cogging torque reduction in a permanent magnet wind turbine generator." In Proc. of the 21 st American Society of Mechanical Engineers Wind Energy Symposium, pp. 1-8. 2002.

[101]Wu, W., V. S. Ramsden, T. Crawford, and G. Hill. "A low speed, high-torque, direct-drive permanent magnet generator for wind turbines." In Industry Applications Conference, 2000. Conference Record of the 2000 IEEE, vol. 1, pp. 147-154. IEEE, 2000.

[102]Zhu, Z. Q., and David Howe. "Influence of design parameters on cogging torque in permanent magnet machines." Energy Conversion, IEEE Transactions on 15, no. 4 (2000): 407-412.

[103]Data of a variable speed wind turbine 450 KW rated power, three phase permanent magnetic type 440/660 V 60 Hz. Provided by Dr. Kathryn, Colorado School of Mines, 2013.